Static, free vibration and buckling analysis of isotropic and sandwich functionally graded plates using a quasi-3D higher-order shear deformation theory and a meshless technique.

Static, free vibration and buckling analysis of functionally graded plates using a quasi-3D higher-order shear deformation theory and a meshless technique

A. M. A. Neves [a], A. J. M. Ferreira [b], E. Carrera [d], M. Cinefra [d], C. M. C. Roque [c], R. M. N. Jorge [a], C. M. M. Soares [e]

[a] *Departamento de Engenharia Mecânica, Faculdade de Engenharia, Universidade do Porto, Rua Dr. Roberto Frias, 4200-465 Porto, Portugal*

[b] *(Corresponding author: ferreira@fe.up.pt)*
Departamento de Engenharia Mecânica, Faculdade de Engenharia, Universidade do Porto, Rua Dr. Roberto Frias, 4200-465 Porto, Portugal

[c] *INEGI, Faculdade de Engenharia, Universidade do Porto, Rua Dr. Roberto Frias, 4200-465 Porto, Portugal*

[d] *Departament of Aeronautics and Aerospace Engineering, Politecnico di Torino, Corso Duca degli Abruzzi, 24, 10129 Torino, Italy*

[e] *Instituto Superior Técnico, Av. Rovisco Pais, Lisboa, Portugal*

Abstract

In this paper the authors derive a higher-order shear deformation theory for modelling functionally graded plates accounting for extensibility in the thickness direction.

The explicit governing equations and boundary conditions are obtained using the principle of virtual displacements under Carrera's Unified Formulation and then interpolated by collocation with radial basis functions.

The efficiency of the present approach is assessed with numerical results including deflection, stresses, free vibration, and buckling of functionally graded isotropic plates and functionally graded sandwich plates.

1 Introduction

Composite materials have been widely used in aircraft and other engineering applications for many years because of their excellent strength-to-weight and

stiffness-to-weight ratios. Functionally graded materials (FGM) are a class of composite materials that were first proposed by Bever and Duwez [1] in 1972. In a typical FGM plate the material properties continuously vary over the thickness direction by mixing two different materials [2], usually ceramic and metal. The gradual variation of properties avoids the delamination failure that are common in laminated composites. The computational modelling of FGM is an important tool to the understanding of the structures behavior, and has been the target of intense research, from micro to macro mechanics [3–6]. A review of the main developments in FGM can be found in Birman and Byrd [7]. These materials have attracted much attention and already have applications in many fields [2] or [8].

When compared to isotropic and laminated plates, the literature on FGM plates is scarce. Because of FGM applications in high temperature environments most of the studies on the behaviour of FGM plates focus on the thermo-mechanical response of FGM plates: Reddy and Chin [9], Reddy [10], Vel and Batra [11,12], Cheng and Batra [13], Javaheri and Eslami [14]. Studies on the mechanical behaviour of FGM plates include the static analysis of FGM plates performed by Kashtalyan [15], Kashtalyan and Menshykova [16], Qian et al. [17], Zenkour [18,19], Ramirez et al. [20], Ferreira et al. [21,22], Chi and Chung [23,24], and Cheng and Batra [25]. Vibrations problems of FGM plates can be found in Batra and Jin [26], Ferreira et al. [27], Vel and Batra [28], Zenkour [29], Roque et al. [30], and Cheng and Batra [31]. Mechanical buckling of FGM plates can be found in Najafizadeh and Eslami [32], Zenkour [29], Cheng and Batra [31], Birman [33], Javaheri and Eslami [34].

The classical plate theory (CLPT) yields acceptable results only for thin plates. The accuracy of the results from the first-order shear deformation theory (FSDT) depends on the shear correction factor which is hard to find as it depends on many parameters. Besides, higher-order shear deformation theories (HSDT) provide better accuracy for transverse shear stresses and there is no need of a shear correction factor. Therefore, we are now proposing a higher-order shear deformation theory based on the following displcament field:

$$\begin{aligned} u &= u_0 + zu_1 + z^3u_3 \\ v &= v_0 + zv_1 + z^3v_3 \\ w &= w_0 + zw_1 + z^2w_2 \end{aligned} \tag{1}$$

A higher-order plate theory popular in the literature is the one from Kant [35], used by Pandya and Kant for laminated plates [36,37], with 6 unknowns. Comparing Kant's theory with present theory, both accounts for warping of the cross section but Kant's theory does not account for the displacements along the coordinate lines of a point on the reference plane (u_0 and v_0) or the rotation w_1. Other popular HSDT are used for laminated plates in [38–40],

with 9 to 12 unknowns depending on the number of terms in the transverse displacement expansion, considering or not warping in the thickness direction. The higher-order presented in this paper includes less unknows in the u and v expansion. Another popular HSDT plate theory in the literature is the one from Reddy [10], with 5 unknowns, already used for FGM plates, but that does not account for warping in the thickness direction unlike present higher-order theory. Although Reddy's theory has 4 unknows less than present theory, the present theory is much easier to implement as it is possible to use the Unified Formulation proposed by Carrera.

Carrera's Unified Formulation (CUF) was proposed in [41–43] for laminated plates and shells and extended to FGM plates in [44–46]. The present formulation can be seen as a generalization of the original CUF, by introducing different displacement fields for in-plane and out-of-plane displacements. It is possible to implement any C_z^0 theory under CUF, using layer-wise as well as equivalent single-layer descriptions, and the Principle of Virtual Displacements, as is the case in present formulation, or the Reissner mixed variational theorem. CUF allows a systematic assessment of a large number of plate models and the effect of thickness stretching in FGM plates was recently investigated by Carrera et al. [47] using CUF and finite element approximations.

The use of alternative methods to the Finite Element Methods for the analysis of plates, such as the meshless methods based on collocation with radial basis functions is atractive due to the absence of a mesh and the ease of collocation methods. In recent years, radial basis functions (RBFs) showed excellent accuracy in the interpolation of data and functions. The authors have applied the RBF collocation to the static deformations and free vibrations of composite beams and plates [48–55]. The combination of CUF and meshless methods has been performed in [56–59] for laminated plates and in [60,61] for FGM plates. Furthermore, the CUF method is here applied for the first time to the buckling analysis of FGM plates, owing to collocation with radial basis functions.

This paper presents explicit governing equations and boundary conditions of the HSDT and focus on the thickness stretching issue on the static, free vibration, and buckling analysis of FGM plates by a meshless technique. The CUF method is employed to obtain the algebraic governing equations and boundary conditions which are then interpolated by radial basis functions to obtain an algebraic system of equations.

2 Problem formulation

Consider a rectangular plate of plan-form dimensions a and b and uniform thickness h. The co-ordinate system is taken such that the x-y plane ($z = 0$)

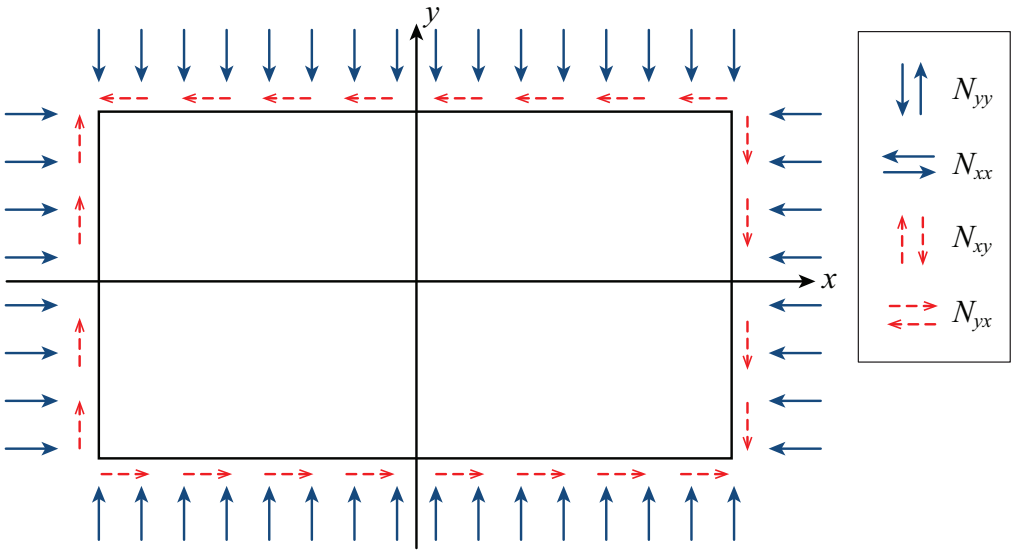

Fig. 1. Rectangular plate subjected to compressive in-plane forces and distributed shear forces.

coincides with the midplane of the plate ($z \in [-h/2, h/2]$).

The plate may be subjected to a transverse mechanical load applied at the top of the plate.

The plate may be subjected to compressive in-plane forces acting on the midplane of the plate and distributed shear force (see fig. 1). $\bar{N}_{xx}$ and $\bar{N}_{yy}$ denote the in-plane loads perpendicular to the edges $x = 0$ and $y = 0$ respectively, and $\bar{N}_{xy}$ denote the distributed shear force parallel to the edges $x = 0$ and $y = 0$ respectively.

We are interested in study three different types of functionally graded plates: (A) isotropic FGM plates; (B) sandwich plates with FGM core; (C) sandwich plates with FGM skins.

2.1 Plate A: isotropic FGM plate

The plate of type A is graded from metal (bottom) to ceramic (top) (see figure 2). The volume fraction of the ceramic phase is defined as in [19]:

$$V_c = \left(0.5 + \frac{z}{h}\right)^p \tag{2}$$

where $z \in [-h/2, h/2]$, h is the thickness of the plate, and p is a scalar parameter that allows the user to define gradation of material properties across the thickness direction. The volume fraction for the metal phase is given as $V_m = 1 - V_c$.

Fig. 2. Plate A: isotropic FGM plate.

Fig. 3. Plate B: sandwich plate with FGM core and isotropic skins.

2.2 Plate B: sandwich plate with FGM core

In this type of sandwich plates the bottom skin is isotropic fully metal and the top skin is isotropic fully ceramic. The core is graded from metal to ceramic so that there are no interfaces between core and skins. Figure 3 illustrates the plate B type.

The volume fraction of the ceramic phase in the core is obtained by adapting the polynomial material law in [19]:

$$V_c = \left(0.5 + \frac{z_c}{h_c}\right)^p \tag{3}$$

where $z_c \in [h_1, h_2]$, $h_c = h_2 - h_1$ is the thickness of the core, and p is the power-law exponent that defines the gradation of material properties across the thickness direction. The volume fraction for the metal phase in the core is given as $V_m = 1 - V_c$.

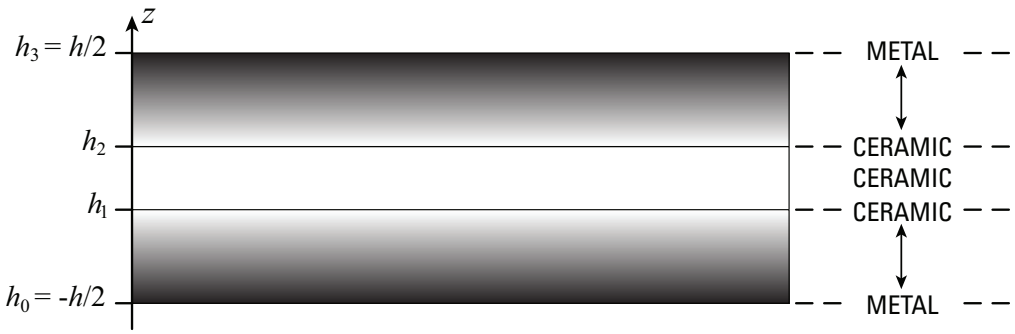

Fig. 4. Plate C: Sandwich with isotropic core and FGM skins.

2.3 Plate C: sandwich plate with FGM skins

In the plates of type C the sandwich core is isotropic fully ceramic and skins are composed of a functionally graded material across the thickness direction. The bottom skin varies from a metal-rich surface ($z = -h/2$) to a ceramic-rich surface while the top skin face varies from a ceramic-rich surface to a metal-rich surface ($z = h/2$) as illustrated in figure 4. There are no interfaces between core and skins. The volume fraction of the ceramic phase is obtained as:

$$\begin{aligned} V_c &= \left(\frac{z - h_0}{h_1 - h_0}\right)^p, \quad h \in [-h/2, h_1], \quad \text{bottom skin} \\ V_c &= 1, \quad h \in [h_1, h_2], \quad \text{core} \\ V_c &= \left(\frac{z - h_3}{h_2 - h_3}\right)^p, \quad h \in [h_2, h/2], \quad \text{top skin} \end{aligned} \tag{4}$$

where $z \in [-h/2, h/2]$, and p is a scalar parameter that allows the user to define gradation of material properties across the thickness direction of the skins. The volume fraction for the metal phase is given as $V_m = 1 - V_c$.

The sandwich plate C may be symmetric or non-symmetric about the mid-plane as we may vary the thickness of each face. Figure 5 shows a non-symmetric sandwich with volume fraction defined by the power-law (4) for various exponents p, in which top skin thickness is the same as the core thickness and the bottom skin thickness is twice the core thickness. Such thickness relation is denoted as 2-1-1. A bottom-core-top notation is being used. 1-1-1 means that skins and core have the same thickness.

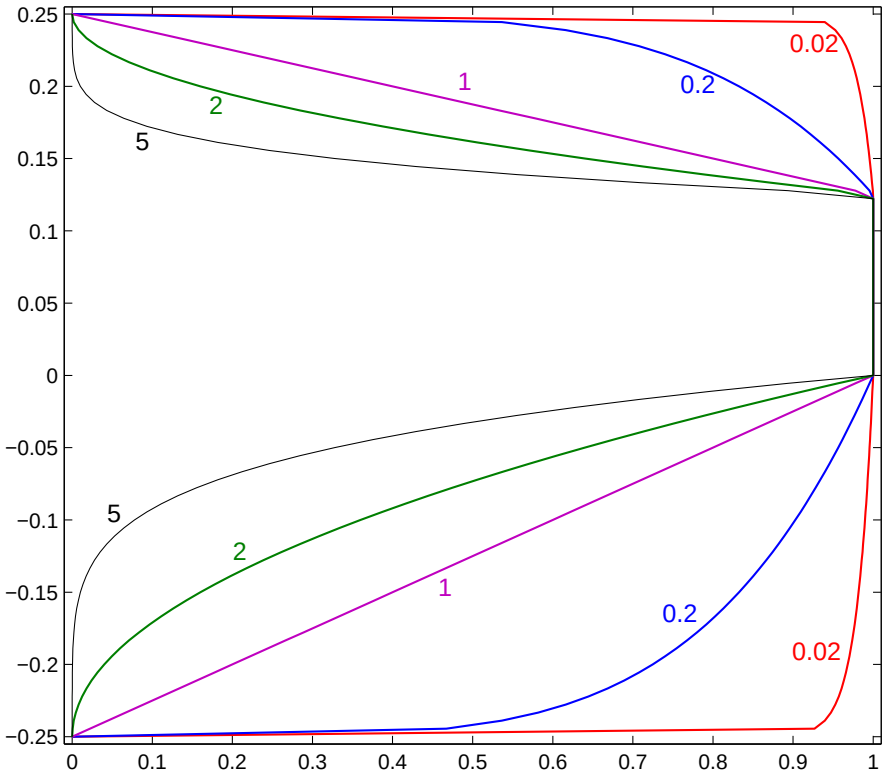

Fig. 5. A 2-1-1 sandwich with FGM skins for several volume fractions.

3 A quasi-3D higher-order plate theory

3.1 Displacement field

The present theory is based on the following displacement field:

$$u(x,y,z,t) = u_0(x,y,t) + zu_1(x,y,t) + z^3u_3(x,y,t) \tag{5}$$

$$v(x,y,z,t) = v_0(x,y,t) + zv_1(x,y,t) + z^3v_3(x,y,t) \tag{6}$$

$$w(x,y,z,t) = w_0(x,y,t) + zw_1(x,y,t) + z^2w_2(x,y,t) \tag{7}$$

where u, v, and w are the displacements in the $x-$, $y-$, and $z-$ directions, respectively. u_0, u_1, u_3, v_0, v_1, v_3, w_0, w_1, and w_2 are functions to be determined.

3.2 Strains

The strain-displacement relationships are given as:

$$\left\{\begin{array}{c}\epsilon_{xx}\\ \epsilon_{yy}\\ \gamma_{xy}\end{array}\right\} = \left\{\begin{array}{c}\frac{\partial u}{\partial x}+\frac{1}{2}\left(\frac{\partial w_0}{\partial x}\right)^2\\ \frac{\partial v}{\partial y}+\frac{1}{2}\left(\frac{\partial w_0}{\partial y}\right)^2\\ \frac{\partial u}{\partial y}+\frac{\partial v}{\partial x}+\frac{\partial w_0}{\partial x}\frac{\partial w_0}{\partial y}\end{array}\right\}, \quad \left\{\begin{array}{c}\gamma_{xz}\\ \gamma_{yz}\\ \epsilon_{zz}\end{array}\right\} = \left\{\begin{array}{c}\frac{\partial u}{\partial z}+\frac{\partial w}{\partial x}\\ \frac{\partial v}{\partial z}+\frac{\partial w}{\partial y}\\ \frac{\partial w}{\partial z}\end{array}\right\} \tag{8}$$

By substitution of the displacement field in (8), the strains are obtained:

$$\left\{\begin{array}{c}\epsilon_{xx}\\ \epsilon_{yy}\\ \gamma_{xy}\end{array}\right\} = \left\{\begin{array}{c}\epsilon_{xx}^{(0)}\\ \epsilon_{yy}^{(0)}\\ \gamma_{xy}^{(0)}\end{array}\right\} + \left\{\begin{array}{c}\epsilon_{xx}^{(nl)}\\ \epsilon_{yy}^{(nl)}\\ \gamma_{xy}^{(nl)}\end{array}\right\} + z\left\{\begin{array}{c}\epsilon_{xx}^{(1)}\\ \epsilon_{yy}^{(1)}\\ \gamma_{xy}^{(1)}\end{array}\right\} + z^3\left\{\begin{array}{c}\epsilon_{xx}^{(3)}\\ \epsilon_{yy}^{(3)}\\ \gamma_{xy}^{(3)}\end{array}\right\} \tag{9}$$

$$\left\{\begin{array}{c}\gamma_{xz}\\ \gamma_{yz}\\ \epsilon_{zz}\end{array}\right\} = \left\{\begin{array}{c}\gamma_{xz}^{(0)}\\ \gamma_{yz}^{(0)}\\ \epsilon_{zz}^{(0)}\end{array}\right\} + z\left\{\begin{array}{c}\gamma_{xz}^{(1)}\\ \gamma_{yz}^{(1)}\\ \epsilon_{zz}^{(1)}\end{array}\right\} + z^2\left\{\begin{array}{c}\gamma_{xz}^{(2)}\\ \gamma_{yz}^{(2)}\\ \epsilon_{zz}^{(2)}\end{array}\right\} \tag{10}$$

being the strain components obtained as

$$\left\{\begin{array}{c}\epsilon_{xx}^{(0)}\\ \epsilon_{yy}^{(0)}\\ \gamma_{xy}^{(0)}\end{array}\right\} = \left\{\begin{array}{c}\frac{\partial u_0}{\partial x}\\ \frac{\partial v_0}{\partial y}\\ \frac{\partial u_0}{\partial y}+\frac{\partial v_0}{\partial x}\end{array}\right\}; \quad \left\{\begin{array}{c}\epsilon_{xx}^{(nl)}\\ \epsilon_{yy}^{(nl)}\\ \gamma_{xy}^{(nl)}\end{array}\right\} = \left\{\begin{array}{c}\frac{1}{2}\left(\frac{\partial w_0}{\partial x}\right)^2\\ \frac{1}{2}\left(\frac{\partial w_0}{\partial y}\right)^2\\ \frac{\partial w_0}{\partial x}\frac{\partial w_0}{\partial y}\end{array}\right\} \tag{11}$$

$$\left\{\begin{array}{c}\epsilon_{xx}^{(1)}\\ \epsilon_{yy}^{(1)}\\ \gamma_{xy}^{(1)}\end{array}\right\} = \left\{\begin{array}{c}\frac{\partial u_1}{\partial x}\\ \frac{\partial v_1}{\partial y}\\ \frac{\partial u_1}{\partial y}+\frac{\partial v_1}{\partial x}\end{array}\right\}; \quad \left\{\begin{array}{c}\epsilon_{xx}^{(3)}\\ \epsilon_{yy}^{(3)}\\ \gamma_{xy}^{(3)}\end{array}\right\} = \left\{\begin{array}{c}\frac{\partial u_3}{\partial x}\\ \frac{\partial v_3}{\partial y}\\ \frac{\partial u_3}{\partial y}+\frac{\partial v_3}{\partial x}\end{array}\right\} \tag{12}$$

$$\left\{\begin{array}{c}\gamma_{xz}^{(0)}\\ \gamma_{yz}^{(0)}\\ \epsilon_{zz}^{(0)}\end{array}\right\} = \left\{\begin{array}{c}u_1+\frac{\partial w_0}{\partial x}\\ v_1+\frac{\partial w_0}{\partial y}\\ w_1\end{array}\right\}; \quad \left\{\begin{array}{c}\gamma_{xz}^{(1)}\\ \gamma_{yz}^{(1)}\\ \epsilon_{zz}^{(1)}\end{array}\right\} = \left\{\begin{array}{c}\frac{\partial w_1}{\partial x}\\ \frac{\partial w_1}{\partial y}\\ 2w_2\end{array}\right\}; \quad \left\{\begin{array}{c}\gamma_{xz}^{(2)}\\ \gamma_{yz}^{(2)}\\ \epsilon_{zz}^{(2)}\end{array}\right\} = \left\{\begin{array}{c}3u_3+\frac{\partial w_2}{\partial x}\\ 3v_3+\frac{\partial w_2}{\partial y}\\ 0\end{array}\right\} \tag{13}$$

where $\epsilon_{\alpha\beta}^{(nl)}$ contains the non-linear terms that will originate the linearized buckling equation.

3.3 Elastic stress-strain relations

In the case of functionally graded materials, the 3D constitutive equations can be written as:

$$\begin{Bmatrix} \sigma_{xx} \\ \sigma_{yy} \\ \tau_{xy} \\ \tau_{xz} \\ \tau_{yz} \\ \sigma_{zz} \end{Bmatrix} = \begin{Bmatrix} C_{11} & C_{12} & 0 & 0 & 0 & C_{12} \\ C_{12} & C_{11} & 0 & 0 & 0 & C_{12} \\ 0 & 0 & C_{44} & 0 & 0 & 0 \\ 0 & 0 & 0 & C_{44} & 0 & 0 \\ 0 & 0 & 0 & 0 & C_{44} & 0 \\ C_{12} & C_{12} & 0 & 0 & 0 & C_{33} \end{Bmatrix} \begin{Bmatrix} \epsilon_{xx} \\ \epsilon_{yy} \\ \gamma_{xy} \\ \gamma_{xz} \\ \gamma_{yz} \\ \epsilon_{zz} \end{Bmatrix} \tag{14}$$

The computation of the elastic constants C_{ij} depends on which assumption of ϵ_{zz} we consider. If $\epsilon_{zz} = 0$, then C_{ij} are the plane-stress reduced elastic constants:

$$C_{11} = \frac{E}{1-\nu^2}; \quad C_{12} = \nu\frac{E}{1-\nu^2}; \quad C_{44} = G; \quad C_{33} = 0 \tag{15}$$

where E is the modulus of elasticity, ν is the Poisson's ratio, and G is the shear modulus $G = \frac{E}{2(1+\nu)}$.

It is interesting to note that the present theory does not consider the use of shear-correction factors, as would be the case of the first-order shear deformation theory (FSDT).

If $\epsilon_{zz} \neq 0$ (thickness stretching), then C_{ij} are the three-dimensional elastic constants, given by

$$C_{11} = \frac{E(1-\nu^2)}{1-3\nu^2-2\nu^3}, \quad C_{12} = \frac{E(\nu+\nu^2)}{1-3\nu^2-2\nu^3} \tag{16}$$

$$C_{44} = G, \quad C_{33} = \frac{E(1-\nu^2)}{1-3\nu^2-2\nu^3} \tag{17}$$

The governing equations of present theory are derived from the dynamic version of the Principle of Virtual Displacements. The internal virtual work is

$$\begin{aligned}\delta U = \int_{\Omega_0} \Bigg\{ \int_{-h/2}^{h/2} \Big[& \sigma_{xx}\left(\delta\epsilon_{xx}^{(0)} + z\delta\epsilon_{xx}^{(1)} + z^3\delta\epsilon_{xx}^{(3)}\right) + \sigma_{yy}\left(\delta\epsilon_{yy}^{(0)} + z\delta\epsilon_{yy}^{(1)} + z^3\delta\epsilon_{yy}^{(3)}\right) \\ & + \sigma_{xy}\left(\delta\gamma_{xy}^{(0)} + z\delta\gamma_{xy}^{(1)} + z^3\delta\gamma_{xy}^{(3)}\right) + \sigma_{xz}\left(\delta\gamma_{xz}^{(0)} + z\delta\gamma_{xz}^{(1)} + z^2\delta\gamma_{xz}^{(2)}\right) \\ & + \sigma_{yz}\left(\delta\gamma_{yz}^{(0)} + z\delta\gamma_{yz}^{(1)} + z^2\delta\gamma_{yz}^{(2)}\right) + \sigma_{zz}\left(\delta\epsilon_{zz}^{(0)} + z\delta\epsilon_{zz}^{(1)}\right) \Big] dz \Bigg\} dx\, dy\end{aligned} \tag{18}$$

$$\begin{aligned}\delta U = \int_{\Omega_0} \Big(& N_{xx}\delta\epsilon_{xx}^{(0)} + M_{xx}\delta\epsilon_{xx}^{(1)} + R_{xx}\delta\epsilon_{xx}^{(3)} + N_{yy}\delta\epsilon_{yy}^{(0)} + M_{yy}\delta\epsilon_{yy}^{(1)} + R_{yy}\delta\epsilon_{yy}^{(3)} \\ & + N_{xy}\delta\gamma_{xy}^{(0)} + M_{xy}\delta\gamma_{xy}^{(1)} + R_{xy}\delta\gamma_{xy}^{(3)} + Q_{xz}\delta\gamma_{xz}^{(0)} + M_{xz}\delta\gamma_{xz}^{(1)} + R_{xz}\delta\gamma_{xz}^{(2)} \\ & + Q_{yz}\delta\gamma_{yz}^{(0)} + M_{yz}\delta\gamma_{yz}^{(1)} + R_{yz}\delta\gamma_{yz}^{(2)} + Q_{zz}\delta\epsilon_{zz}^{(0)} + M_{zz}\delta\epsilon_{zz}^{(1)}\Big) dx\, dy\end{aligned} \tag{19}$$

where Ω_0 is the integration domain in plane (x, y) and

$$\begin{Bmatrix} N_{xx} \\ N_{yy} \\ N_{xy} \end{Bmatrix} = \int_{-h/2}^{h/2} \begin{Bmatrix} \sigma_{xx} \\ \sigma_{yy} \\ \sigma_{xy} \end{Bmatrix} dz, \quad \begin{Bmatrix} Q_{xz} \\ Q_{yz} \\ Q_{zz} \end{Bmatrix} = \int_{-h/2}^{h/2} \begin{Bmatrix} \sigma_{xz} \\ \sigma_{yz} \\ \sigma_{zz} \end{Bmatrix} dz \tag{20}$$

$$\begin{Bmatrix} M_{xx} \\ M_{yy} \\ M_{xy} \end{Bmatrix} = \int_{-h/2}^{h/2} z \begin{Bmatrix} \sigma_{xx} \\ \sigma_{yy} \\ \sigma_{xy} \end{Bmatrix} dz, \quad \begin{Bmatrix} M_{xz} \\ M_{yz} \\ M_{zz} \end{Bmatrix} = \int_{-h/2}^{h/2} z \begin{Bmatrix} \sigma_{xz} \\ \sigma_{yz} \\ \sigma_{zz} \end{Bmatrix} dz \tag{21}$$

$$\begin{Bmatrix} R_{xx} \\ R_{yy} \\ R_{xy} \end{Bmatrix} = \int_{-h/2}^{h/2} z^3 \begin{Bmatrix} \sigma_{xx} \\ \sigma_{yy} \\ \sigma_{xy} \end{Bmatrix} dz, \quad \begin{Bmatrix} R_{xz} \\ R_{yz} \end{Bmatrix} = \int_{-h/2}^{h/2} z^2 \begin{Bmatrix} \sigma_{xz} \\ \sigma_{yz} \end{Bmatrix} dz. \tag{22}$$

The external virtual work due to external loads applied to the plate is given

as:

$$\begin{aligned}\delta V &= -\int_{\Omega_0} \left(p_x \delta u + p_y \delta v + p_z \delta w\right) dx\ dy \\ &= -\int_{\Omega_0} \left(p_x \left(\delta u_0 + z\delta u_1 + z^3 \delta u_3\right) + p_y \left(\delta v_0 + z\delta v_1 + z^3 \delta v_3\right) + p_z \left(\delta w_0 + z\delta w_1 + z^2 \delta w_2\right)\right) dx\ dy\end{aligned} \tag{23}$$

The external virtual work due to in-plane forces and shear forces applied to the plate is given as:

$$\delta V = -\int_{\Omega_0} \left[\bar{N}_{xx} \frac{\partial w_0}{\partial x} \frac{\delta \partial w_0}{\partial x} + \bar{N}_{xy} \frac{\partial w_0}{\partial y} \frac{\delta \partial w_0}{\partial x} + \bar{N}_{yx} \frac{\partial w_0}{\partial x} \frac{\delta \partial w_0}{\partial y} + \bar{N}_{yy} \frac{\partial w_0}{\partial y} \frac{\delta \partial w_0}{\partial y}\right] dx\ dy \tag{24}$$

being $\bar{N}_{xx}$ and $\bar{N}_{yy}$ the in-plane loads perpendicular to the edges $x = 0$ and $y = 0$ respectively, and $\bar{N}_{xy}$ and $\bar{N}_{yx}$ the distributed shear forces parallel to the edges $x = 0$ and $y = 0$ respectively.

The virtual kinetic energy is given as:

$$\begin{aligned}\delta K =& \int_{\Omega_0} \left\{ \int_{-h/2}^{h/2} \rho \left(\dot{u}\delta\dot{u} + \dot{v}\delta\dot{v} + \dot{w}\delta\dot{w}\right) dz \right\} dx\ dy \\ =& \int_{\Omega_0} \left\{ \int_{-h/2}^{h/2} \rho \Big[\left(\dot{u}_0\delta\dot{u}_0 + \dot{v}_0\delta\dot{v}_0 + \dot{w}_0\delta\dot{w}_0\right) \right. \\ &+ z\left(\dot{u}_0\delta\dot{u}_1 + \dot{u}_1\delta\dot{u}_0 + \dot{v}_0\delta\dot{v}_1 + \dot{v}_1\delta\dot{v}_0 + \dot{w}_0\delta\dot{w}_1 + \dot{w}_1\delta\dot{w}_0\right) \\ &+ z^2\left(\dot{u}_1\delta\dot{u}_1 + \dot{v}_1\delta\dot{v}_1 + \dot{w}_0\delta\dot{w}_2 + \dot{w}_1\delta\dot{w}_1 + \dot{w}_2\delta\dot{w}_0\right) \\ &+ z^3\left(\dot{u}_0\delta\dot{u}_3 + \dot{u}_3\delta\dot{u}_0 + \dot{v}_0\delta\dot{v}_3 + \dot{v}_3\delta\dot{v}_0 + \dot{w}_1\delta\dot{w}_2 + \dot{w}_2\delta\dot{w}_1\right) \\ &+ z^4\left(\dot{u}_1\delta\dot{u}_3 + \dot{u}_3\delta\dot{u}_1 + \dot{v}_3\delta\dot{v}_1 + \dot{v}_1\delta\dot{v}_3 + \dot{w}_2\delta\dot{w}_2\right) \\ &\left. + z^6\left(\dot{u}_3\delta\dot{u}_3 + \dot{v}_3\delta\dot{v}_3\right) \Big] dz \right\} dx\ dy\end{aligned} \tag{25}$$

$$\begin{aligned}\delta K =& \int_{\Omega_0} \Big[I_0 \left(\dot{u}_0\delta\dot{u}_0 + \dot{v}_0\delta\dot{v}_0 + \dot{w}_0\delta\dot{w}_0\right) \\ &+ I_1\left(\dot{u}_0\delta\dot{u}_1 + \dot{u}_1\delta\dot{u}_0 + \dot{v}_0\delta\dot{v}_1 + \dot{v}_1\delta\dot{v}_0 + \dot{w}_0\delta\dot{w}_1 + \dot{w}_1\delta\dot{w}_0\right) \\ &+ I_2\left(\dot{u}_1\delta\dot{u}_1 + \dot{v}_1\delta\dot{v}_1 + \dot{w}_0\delta\dot{w}_2 + \dot{w}_1\delta\dot{w}_1 + \dot{w}_2\delta\dot{w}_0\right) \\ &+ I_3\left(\dot{u}_0\delta\dot{u}_3 + \dot{u}_3\delta\dot{u}_0 + \dot{v}_0\delta\dot{v}_3 + \dot{v}_3\delta\dot{v}_0 + \dot{w}_1\delta\dot{w}_2 + \dot{w}_2\delta\dot{w}_1\right) \\ &+ I_4\left(\dot{u}_1\delta\dot{u}_3 + \dot{u}_3\delta\dot{u}_1 + \dot{v}_3\delta\dot{v}_1 + \dot{v}_1\delta\dot{v}_3 + \dot{w}_2\delta\dot{w}_2\right) \\ &+ I_6\left(\dot{u}_3\delta\dot{u}_3 + \dot{v}_3\delta\dot{v}_3\right) \Big] dx\ dy\end{aligned} \tag{26}$$

where the dots denote the derivative with respect to time t and the inertia

terms are defined as

$$I_i = \int_{-h/2}^{h/2} \rho z^i dz \quad i = 1, 2, 3, 4, 6 \tag{27}$$

Substituting δU, δV, and δK in the virtual work statement, integrating through the thickness, integrating by parts with respect to x and y, and collecting the coefficients of $\delta \boldsymbol{u}_0$, $\delta \boldsymbol{u}_1$, $\delta \boldsymbol{u}_3$, $\delta \boldsymbol{v}_0$, $\delta \boldsymbol{v}_1$, $\delta \boldsymbol{v}_3$, $\delta \boldsymbol{w}_0$, $\delta \boldsymbol{w}_1$, $\delta \boldsymbol{w}_2$, the following governing equations are obtained:

$$\begin{aligned}
\delta \boldsymbol{u}_0 &: -\frac{\partial N_{xx}}{\partial x} - \frac{\partial N_{xy}}{\partial y} + \frac{\partial Q_{xz}}{\partial z} = \int_{-h/2}^{h/2} \left\{ \rho \left(\ddot{u}_0 + z\ddot{u}_1 + z^3 \ddot{u}_3 \right) + p_x \right\} dz \\
\delta \boldsymbol{v}_0 &: -\frac{\partial N_{xy}}{\partial x} - \frac{\partial N_{yy}}{\partial y} + \frac{\partial Q_{yz}}{\partial z} = \int_{-h/2}^{h/2} \left\{ \rho \left(\ddot{v}_0 + z\ddot{v}_1 + z^3 \ddot{v}_3 \right) + p_y \right\} dz \\
\delta \boldsymbol{w}_0 &: -\frac{\partial Q_{xz}}{\partial x} - \frac{\partial Q_{yz}}{\partial y} + \frac{\partial Q_{zz}}{\partial z} + \bar{N}_{xx} \frac{\partial^2 w_0}{\partial x^2} + \bar{N}_{xy} \frac{\partial^2 w_0}{\partial y \partial x} + \bar{N}_{yx} \frac{\partial^2 w_0}{\partial x \partial y} \\
&\quad + \bar{N}_{yy} \frac{\partial^2 w_0}{\partial y^2} = \int_{-h/2}^{h/2} \left\{ \rho \left(\ddot{w}_0 + z\ddot{w}_1 + z^2 \ddot{w}_2 \right) + p_z \right\} dz \\
\delta \boldsymbol{u}_1 &: -\frac{\partial M_{xx}}{\partial x} - \frac{\partial M_{xy}}{\partial y} + \frac{\partial M_{xz}}{\partial z} = \int_{-h/2}^{h/2} \left\{ \rho z \left(\ddot{u}_0 + z\ddot{u}_1 + z^3 \ddot{u}_3 \right) + z p_x \right\} dz \\
\delta \boldsymbol{v}_1 &: -\frac{\partial M_{xy}}{\partial x} - \frac{\partial M_{yy}}{\partial y} + \frac{\partial M_{yz}}{\partial z} = \int_{-h/2}^{h/2} \left\{ \rho z \left(\ddot{v}_0 + z\ddot{v}_1 + z^3 \ddot{v}_3 \right) + z p_y \right\} dz \\
\delta \boldsymbol{w}_1 &: -\frac{\partial M_{xz}}{\partial x} - \frac{\partial M_{yz}}{\partial y} + \frac{\partial M_{zz}}{\partial z} = \int_{-h/2}^{h/2} \left\{ \rho z \left(\ddot{w}_0 + z\ddot{w}_1 + z^2 \ddot{w}_2 \right) + z p_z \right\} dz \\
\delta \boldsymbol{u}_3 &: -\frac{\partial R_{xx}}{\partial x} - \frac{\partial R_{xy}}{\partial y} + \frac{\partial R_{xz}}{\partial z} = \int_{-h/2}^{h/2} \left\{ \rho z^3 \left(\ddot{u}_0 + z\ddot{u}_1 + z^3 \ddot{u}_3 \right) + z^3 p_x \right\} dz \\
\delta \boldsymbol{v}_3 &: -\frac{\partial R_{xy}}{\partial x} - \frac{\partial R_{yy}}{\partial y} + \frac{\partial R_{yz}}{\partial z} = \int_{-h/2}^{h/2} \left\{ \rho z^3 \left(\ddot{v}_0 + z\ddot{v}_1 + z^3 \ddot{v}_3 \right) + z^3 p_y \right\} dz \\
\delta \boldsymbol{w}_2 &: -\frac{\partial R_{xz}}{\partial x} - \frac{\partial R_{yz}}{\partial y} + \frac{\partial R_{zz}}{\partial z} = \int_{-h/2}^{h/2} \left\{ \rho z^2 \left(\ddot{w}_0 + z\ddot{w}_1 + z^2 \ddot{w}_2 \right) + z^2 p_z \right\} dz
\end{aligned} \tag{28}$$

The mechanical boundary conditions are:

$$\begin{aligned}
&\delta \boldsymbol{u}_0 : n_x N_{xx} + n_y N_{xy} = n_x \bar{N}_{xx} + n_y \bar{N}_{xy} \\
&\delta \boldsymbol{v}_0 : n_x N_{xy} + n_y N_{yy} = n_x \bar{N}_{xy} + n_y \bar{N}_{yy} \\
&\delta \boldsymbol{w}_0 : n_x Q_{xz} + n_y Q_{yz} = n_x \bar{Q}_{xz} + n_y \bar{Q}_{yz} \\
&\delta \boldsymbol{u}_1 : n_x M_{xx} + n_y M_{xy} = n_x \bar{M}_{xx} + n_y \bar{M}_{xy} \\
&\delta \boldsymbol{v}_1 : n_x M_{xy} + n_y M_{yy} = n_x \bar{M}_{xy} + n_y \bar{M}_{yy} \\
&\delta \boldsymbol{w}_1 : n_x M_{xz} + n_y M_{yz} = n_x \bar{M}_{xz} + n_y \bar{M}_{yz} \\
&\delta \boldsymbol{u}_3 : n_x R_{xx} + n_y R_{xy} = n_x \bar{R}_{xx} + n_y \bar{R}_{xy} \\
&\delta \boldsymbol{v}_3 : n_x R_{xy} + n_y R_{yy} = n_x \bar{R}_{xy} + n_y \bar{R}_{yy} \\
&\delta \boldsymbol{w}_2 : n_x R_{xz} + n_y R_{yz} = n_x \bar{R}_{xz} + n_y \bar{R}_{yz}
\end{aligned} \tag{29}$$

where (n_x, n_y) denotes the unit normal-to-boundary vector.

4 Governing equations and boundary conditions in the framework of Unified Formulation

The Unified Formulation proposed by Carrera [62,42] (further denoted as CUF) has been applied, using the Principle of Virtual Displacements, to obtain the equations of the present theory (see equation (28)). The stiffness matrix components, the external force terms or the inertia terms can be obtained directly with this unified formulation, irrespective of the shear deformation theory being considered.

The three displacement components u_x, u_y and u_z (given in (5) to (7)) and their relative variations can be modelled as:

$$(u_x, u_y, u_z) = F_\tau \left(u_{x\tau}, u_{y\tau}, u_{z\tau}\right) \qquad (\delta u_x, \delta u_y, \delta u_z) = F_s \left(\delta u_{xs}, \delta u_{ys}, \delta u_{zs}\right) \tag{30}$$

In the present formulation the thickness functions are

$$F_{sux} = F_{suy} = F_{\tau ux} = F_{\tau uy} = \begin{bmatrix} 1 & z & z^3 \end{bmatrix} \tag{31}$$

for inplane displacements u, v and

$$F_{suz} = F_{\tau uz} = \begin{bmatrix} 1 & z & z^2 \end{bmatrix} \tag{32}$$

for transverse displacement w.

The CUF formulation considers virtual (mathematical) layers of constant thickness, each containing a homogeneized modulus of elasticity, E^k, and a homogeneized Poisson's ratio, ν^k. The functionally graded plate is divided

into a number (NL) of uniform thickness layers and for each layer the volume fraction of the ceramic phase is defined according to (2), (3) or (4). The volume fraction for the metal phase is given as $V_m = 1 - V_c$.

For each virtual layer, the elastic properties E^k and ν^k can be computed in two ways. First, we may consider the law-of-mistures:

$$E^k(z) = E_m V_m + E_c V_c; \qquad \nu^k(z) = \nu_m V_m + \nu_c V_c \tag{33}$$

Second, we may consider the Mori-Tanaka homogenization procedure [63,64]. In this homogenization method, we find the bulk modulus, K, and the effective shear modulus, G, of the composite equivalent layer as

$$\frac{K - K_m}{K_c - K_m} = \frac{V_c}{1 + V_m \frac{K_c - K_m}{K_m + 4/3 G_m}}; \quad \frac{G - G_m}{G_c - G_m} = \frac{V_c}{1 + V_m \frac{G_c - G_m}{G_m + f_m}} \tag{34}$$

where

$$f_m = \frac{G_m(9K_m + 8G_m)}{6(K_m + 2G_m)} \tag{35}$$

The effective values of Young's modulus, E^k, and Poisson's ratio, ν^k, are found from

$$E^k = \frac{9KG}{3K + G}; \quad \nu^k = \frac{3K - 2G}{2(3K + G)} \tag{36}$$

After using the law-of-mixtures or the Mori-Tanaka homogenization procedure, the computation of the elastic constants C_{ij}^k is performed for each layer based on ν^k and E^k. For example,

$$C_{12}^k = \frac{E^k(\nu^k + (\nu^k)^2)}{1 - 3(\nu^k)^2 - 2(\nu^k)^3}. \tag{37}$$

The procedure for the other C_{ij}^k is analogous.

Under CUF formulation the PVD is expressed considering a sumatoria over the layers:

$$\sum_{k=1}^{NL} \int_{\Omega_k} \int_{A_k} \left(\delta {\boldsymbol{\epsilon}_p}^T \boldsymbol{\sigma}_p^k + \delta {\boldsymbol{\epsilon}_n}^T \boldsymbol{\sigma}_n^k \right) dz \, d\Omega_k = \sum_{k=1}^{NL} \int_{\Omega_k} \int_{A_k} \left(\rho^k \, \delta \boldsymbol{u}^T \ddot{\boldsymbol{u}} + \delta \boldsymbol{u}^T \boldsymbol{p} \right) dz \, d\Omega_k \tag{38}$$

Here, k indicates the layer and Ω_k and A_k are the integration domains in plane (x,y) and z direction, respectively, and ρ^k is the mass density of the k-th layer. Subscript p indicates in-plane components (xx, yy, xy) and subscript n the transverse components (xz, yz, and zz). $\boldsymbol{p} = \{p_x, p_y, p_z\}$ is the external load applied to the structure. T denotes the transpose of a vector, δ denotes the variational symbol, and double dots acceleration.

Equation (38) considers the 9 variationals $\delta\boldsymbol{u}_0$, $\delta\boldsymbol{v}_0$, $\delta\boldsymbol{w}_0$, $\delta\boldsymbol{u}_1$, $\delta\boldsymbol{v}_1$, $\delta\boldsymbol{w}_1$, $\delta\boldsymbol{u}_Z$, $\delta\boldsymbol{v}_Z$, and $\delta\boldsymbol{w}_2$ disregarding the the in-plane loads and the shear forces. These external forces just imply addicional terms on the variational $\delta\boldsymbol{w}_0$:

$$\int_{\Omega_0} \bar{N}_{\alpha\beta} w_{0,\alpha} \delta w_{0,\beta} d\Omega_0 \tag{39}$$

where Ω_0 is the integration domain in plane (x, y) and α and β take the symbols x, y.

Considering that the mechanical external load is only transverse $\boldsymbol{p} = \{0, 0, p_z\}$ applied at the top (coordinate $z = h/2$) and assuming that $\bar{N}_{xy} = \bar{N}_{yx}$, equations in (28) become:

$$\begin{aligned}
\delta\boldsymbol{u}_0 &: \sum_{k=1}^{NL} \left(-\frac{\partial N_{xx}^k}{\partial x} - \frac{\partial N_{xy}^k}{\partial y} + \frac{\partial Q_{xz}^k}{\partial z} \right) = \sum_{k=1}^{NL} \int_{A_k} \rho^k \left(\ddot{u}_0 + z\ddot{u}_1 + z^3 \ddot{u}_3 \right) dz \\
\delta\boldsymbol{v}_0 &: \sum_{k=1}^{NL} \left(-\frac{\partial N_{xy}^k}{\partial x} - \frac{\partial N_{yy}^k}{\partial y} + \frac{\partial Q_{yz}^k}{\partial z} \right) = \sum_{k=1}^{NL} \int_{A_k} \rho^k \left(\ddot{v}_0 + z\ddot{v}_1 + z^3 \ddot{v}_3 \right) dz \\
\delta\boldsymbol{w}_0 &: \sum_{k=1}^{NL} \left(-\frac{\partial Q_{xz}^k}{\partial x} - \frac{\partial Q_{yz}^k}{\partial y} + \frac{\partial Q_{zz}^k}{\partial z} \right) + \bar{N}_{xx} \frac{\partial^2 w_0}{\partial x^2} + 2\bar{N}_{xy} \frac{\partial^2 w_0}{\partial x \partial y} + \bar{N}_{yy} \frac{\partial^2 w_0}{\partial y^2} \\
&\quad = \sum_{k=1}^{NL} \int_{A_k} \rho^k \left(\ddot{w}_0 + z\ddot{w}_1 + z^2 \ddot{w}_2 \right) dz + p_z \\
\delta\boldsymbol{u}_1 &: \sum_{k=1}^{NL} \left(-\frac{\partial M_{xx}^k}{\partial x} - \frac{\partial M_{xy}^k}{\partial y} + \frac{\partial M_{xz}^k}{\partial z} \right) = \sum_{k=1}^{NL} \int_{A_k} \rho^k z \left(\ddot{u}_0 + z\ddot{u}_1 + z^3 \ddot{u}_3 \right) dz \\
\delta\boldsymbol{v}_1 &: \sum_{k=1}^{NL} \left(-\frac{\partial M_{xy}^k}{\partial x} - \frac{\partial M_{yy}^k}{\partial y} + \frac{\partial M_{yz}^k}{\partial z} \right) = \sum_{k=1}^{NL} \int_{A_k} \rho^k z \left(\ddot{v}_0 + z\ddot{v}_1 + z^3 \ddot{v}_3 \right) dz \\
\delta\boldsymbol{w}_1 &: \sum_{k=1}^{NL} \left(-\frac{\partial M_{xz}^k}{\partial x} - \frac{\partial M_{yz}^k}{\partial y} + \frac{\partial M_{zz}^k}{\partial z} \right) = \sum_{k=1}^{NL} \int_{A_k} \rho^k z \left(\ddot{w}_0 + z\ddot{w}_1 + z^2 \ddot{w}_2 \right) dz \\
\delta\boldsymbol{u}_3 &: \sum_{k=1}^{NL} \left(-\frac{\partial R_{xx}^k}{\partial x} - \frac{\partial R_{xy}^k}{\partial y} + \frac{\partial R_{xz}^k}{\partial z} \right) = \sum_{k=1}^{NL} \int_{A_k} \rho^k z^3 \left(\ddot{u}_0 + z\ddot{u}_1 + z^3 \ddot{u}_3 \right) dz \\
\delta\boldsymbol{v}_3 &: \sum_{k=1}^{NL} \left(-\frac{\partial R_{xy}^k}{\partial x} - \frac{\partial R_{yy}^k}{\partial y} + \frac{\partial R_{yz}^k}{\partial z} \right) = \sum_{k=1}^{NL} \int_{A_k} \rho^k z^3 \left(\ddot{v}_0 + z\ddot{v}_1 + z^3 \ddot{v}_3 \right) dz \\
\delta\boldsymbol{w}_2 &: \sum_{k=1}^{NL} \left(-\frac{\partial R_{xz}^k}{\partial x} - \frac{\partial R_{yz}^k}{\partial y} + \frac{\partial R_{zz}^k}{\partial z} \right) = \sum_{k=1}^{NL} \int_{A_k} \rho^k z^2 \left(\ddot{w}_0 + z\ddot{w}_1 + z^2 \ddot{w}_2 \right) dz + \left(\frac{h}{2} \right)^2 p_z
\end{aligned} \tag{40}$$

where $N_{xx}^k = \int_{A_k} \sigma_{xx}^k dz$, $R_{xz}^k = \int_{A_k} z^2 \sigma_{xz}^k dz$ and analogous procedure for other resultants.

In (40), for static problems, the ρ^k and the $\bar{N}_{\alpha\beta}$ terms are set to zero; for the free vibration problems, the $\bar{N}_{\alpha\beta}$ and the p_z terms are set to zero; and for buckling problems the p_z and the ρ^k terms are set to zero.

4.1 Governing equations and boundary conditions in terms of displacements

In order to discretize the governing equations by radial basis functions, we present in the following the explicit terms of the governing equations and the boundary conditions in terms of the generalized displacements.

$$\begin{aligned}\delta u_0 : &-\left(A_{11}\frac{\partial^2 u_0}{\partial x^2}+A_{66}\frac{\partial^2 u_0}{\partial y^2}\right)-\left(A_{12}+A_{66}\right)\frac{\partial^2 v_0}{\partial x\partial y}-\left(B_{11}\frac{\partial^2 u_1}{\partial x^2}+B_{66}\frac{\partial^2 u_1}{\partial y^2}\right)\\ &-\left(E_{11}\frac{\partial^2 u_3}{\partial x^2}+E_{66}\frac{\partial^2 u_3}{\partial y^2}\right)-\left(B_{12}+B_{66}\right)\frac{\partial^2 v_1}{\partial x\partial y}-\left(E_{12}+E_{66}\right)\frac{\partial^2 v_3}{\partial x\partial y}\\ &-A_{13}\frac{\partial w_1}{\partial x}-2B_{13}\frac{\partial w_2}{\partial x}=I_0\frac{\partial^2 u_0}{\partial t^2}+I_1\frac{\partial^2 u_1}{\partial t^2}+I_3\frac{\partial^2 u_3}{\partial t^2}\end{aligned} \tag{41}$$

$$\begin{aligned}\delta u_1 : \quad &\left(-F_{11}\frac{\partial^2 u_3}{\partial x^2}+3D_{55}u_3-F_{66}\frac{\partial^2 u_3}{\partial y^2}\right)+\left(-D_{11}\frac{\partial^2 u_1}{\partial x^2}+A_{55}u_1-D_{66}\frac{\partial^2 u_1}{\partial y^2}\right)\\ &-\left(B_{11}\frac{\partial^2 u_0}{\partial x^2}+B_{66}\frac{\partial^2 u_0}{\partial y^2}\right)-\left(B_{12}+B_{66}\right)\frac{\partial^2 v_0}{\partial x\partial y}-\left(D_{12}+D_{66}\right)\frac{\partial^2 v_1}{\partial x\partial y}\\ &-\left(F_{12}+F_{66}\right)\frac{\partial^2 v_3}{\partial x\partial y}+\left(-B_{13}+B_{55}\right)\frac{\partial w_1}{\partial x}+\left(-2D_{13}+D_{55}\right)\frac{\partial w_2}{\partial x}+A_{55}\frac{\partial w_0}{\partial x}\\ =&\, I_1\frac{\partial^2 u_0}{\partial t^2}+I_2\frac{\partial^2 u_1}{\partial t^2}+I_4\frac{\partial^2 u_3}{\partial t^2}\end{aligned} \tag{42}$$

$$\begin{aligned}\delta u_3 : \quad &\left(-F_{11}\frac{\partial^2 u_1}{\partial x^2}+3D_{55}u_1-F_{66}\frac{\partial^2 u_1}{\partial y^2}\right)+\left(-G_{11}\frac{\partial^2 u_3}{\partial x^2}+9F_{55}u_3-G_{66}\frac{\partial^2 u_3}{\partial y^2}\right)\\ &-\left(E_{11}\frac{\partial^2 u_0}{\partial x^2}+E_{66}\frac{\partial^2 u_0}{\partial y^2}\right)-\left(E_{12}+E_{66}\right)\frac{\partial^2 v_0}{\partial x\partial y}-\left(F_{12}+F_{66}\right)\frac{\partial^2 v_1}{\partial x\partial y}\\ &-\left(G_{12}+G_{66}\right)\frac{\partial^2 v_3}{\partial x\partial y}+\left(-E_{13}+3E_{55}\right)\frac{\partial w_1}{\partial x}+\left(-2F_{13}+3F_{55}\right)\frac{\partial w_2}{\partial x}+3D_{55}\frac{\partial w_0}{\partial x}\\ =&\, I_3\frac{\partial^2 u_0}{\partial t^2}+I_4\frac{\partial^2 u_1}{\partial t^2}+I_6\frac{\partial^2 u_3}{\partial t^2}\end{aligned} \tag{43}$$

$$\delta v_0 : -\left(A_{12}+A_{66}\right)\frac{\partial^2 u_0}{\partial x\partial y}-\left(A_{22}\frac{\partial^2 v_0}{\partial y^2}+A_{66}\frac{\partial^2 v_0}{\partial x^2}\right)-\left(B_{12}+B_{66}\right)\frac{\partial^2 u_1}{\partial x\partial y}$$
$$-\left(E_{12}+E_{66}\right)\frac{\partial^2 u_3}{\partial x\partial y}-\left(B_{22}\frac{\partial^2 v_1}{\partial y^2}+B_{66}\frac{\partial^2 v_1}{\partial x^2}\right)-\left(E_{22}\frac{\partial^2 v_3}{\partial y^2}+E_{66}\frac{\partial^2 v_3}{\partial x^2}\right)$$
$$-A_{23}\frac{\partial w_1}{\partial y}-2B_{23}\frac{\partial w_2}{\partial y}=I_0\frac{\partial^2 v_0}{\partial t^2}+I_1\frac{\partial^2 v_1}{\partial t^2}+I_3\frac{\partial^2 v_3}{\partial t^2} \tag{44}$$

$$\delta v_1 : \quad \left(-F_{22}\frac{\partial^2 v_3}{\partial y^2}+3D_{44}v_3-F_{66}\frac{\partial^2 v_3}{\partial x^2}\right)+\left(-D_{22}\frac{\partial^2 v_1}{\partial y^2}+A_{44}v_1-D_{66}\frac{\partial^2 v_1}{\partial x^2}\right)$$
$$-\left(B_{12}+B_{66}\right)\frac{\partial^2 u_0}{\partial x\partial y}-\left(D_{12}+D_{66}\right)\frac{\partial^2 u_1}{\partial x\partial y}-\left(F_{12}+F_{66}\right)\frac{\partial^2 u_3}{\partial x\partial y}$$
$$-\left(B_{22}\frac{\partial^2 v_0}{\partial y^2}+B_{66}\frac{\partial^2 v_0}{\partial x^2}\right)+\left(-B_{23}+B_{44}\right)\frac{\partial w_1}{\partial y}+\left(-2D_{23}+D_{44}\right)\frac{\partial w_2}{\partial y}+A_{44}\frac{\partial w_0}{\partial y}$$
$$=I_1\frac{\partial^2 v_0}{\partial t^2}+I_2\frac{\partial^2 v_1}{\partial t^2}+I_4\frac{\partial^2 v_3}{\partial t^2} \tag{45}$$

$$\delta v_3 : \quad \left(-F_{22}\frac{\partial^2 v_1}{\partial y^2}+3D_{44}v_1-F_{66}\frac{\partial^2 v_1}{\partial x^2}\right)+\left(-G_{22}\frac{\partial^2 v_3}{\partial y^2}+9F_{44}v_3-G_{66}\frac{\partial^2 v_3}{\partial x^2}\right)$$
$$-\left(E_{12}+E_{66}\right)\frac{\partial^2 u_0}{\partial x\partial y}-\left(F_{12}+F_{66}\right)\frac{\partial^2 u_1}{\partial x\partial y}-\left(G_{12}+G_{66}\right)\frac{\partial^2 u_3}{\partial x\partial y}$$
$$-\left(E_{22}\frac{\partial^2 v_0}{\partial y^2}+E_{66}\frac{\partial^2 v_0}{\partial x^2}\right)+\left(-E_{23}+3E_{44}\right)\frac{\partial w_1}{\partial y}+\left(-2F_{23}+3F_{44}\right)\frac{\partial w_2}{\partial y}+3D_{44}\frac{\partial w_0}{\partial y}$$
$$=I_3\frac{\partial^2 v_0}{\partial t^2}+I_4\frac{\partial^2 v_1}{\partial t^2}+I_6\frac{\partial^2 v_3}{\partial t^2} \tag{46}$$

$$\delta w_0 : -\left(A_{55}\frac{\partial^2 w_0}{\partial x^2}+A_{44}\frac{\partial^2 w_0}{\partial y^2}\right)-\left(B_{55}\frac{\partial^2 w_1}{\partial x^2}+B_{44}\frac{\partial^2 w_1}{\partial y^2}\right)-\left(D_{55}\frac{\partial^2 w_2}{\partial x^2}+D_{44}\frac{\partial^2 w_2}{\partial y^2}\right)$$
$$-A_{55}\frac{\partial u_1}{\partial x}-A_{44}\frac{\partial v_1}{\partial y}-3D_{55}\frac{\partial u_3}{\partial x}-3D_{44}\frac{\partial v_3}{\partial y} \tag{47}$$
$$+\bar{N}_{xx}\frac{\partial^2 w_0}{\partial x^2}+2\bar{N}_{xy}\frac{\partial^2 w_0}{\partial x\partial y}+\bar{N}_{yy}\frac{\partial^2 w_0}{\partial y^2}=I_0\frac{\partial^2 w_0}{\partial t^2}+I_1\frac{\partial^2 w_1}{\partial t^2}+I_2\frac{\partial^2 w_2}{\partial t^2}+p_z \tag{48}$$

$$\delta w_1 : \left(-E_{55}\frac{\partial^2 w_2}{\partial x^2} + 2B_{33}w_2 - E_{44}\frac{\partial^2 w_2}{\partial y^2 w_2}\right) + \left(-D_{55}\frac{\partial^2 w_1}{\partial x^2} + A_{33}w_1 - D_{44}\frac{\partial^2 w_1}{\partial y^2}\right)$$
$$+ (B_{13} - B_{55})\frac{\partial u_1}{\partial x} + (E_{13} - 3E_{55})\frac{\partial u_3}{\partial x} + (B_{23} - B_{44})\frac{\partial v_1}{\partial y} + (E_{23} - 3E_{44})\frac{\partial v_3}{\partial y}$$
$$- \left(B_{55}\frac{\partial^2 w_0}{\partial x^2} + B_{44}\frac{\partial^2 w_0}{\partial y^2}\right) + A_{13}\frac{\partial u_0}{\partial x} + A_{23}\frac{\partial v_0}{\partial y} = I_1\frac{\partial^2 w_0}{\partial t^2} + I_2\frac{\partial^2 w_1}{\partial t^2} + I_3\frac{\partial^2 w_2}{\partial t^2} \tag{49}$$

$$\delta w_2 : \left(-E_{55}\frac{\partial^2 w_1}{\partial x^2} + 2B_{33}w_1 - E_{44}\frac{\partial^2 w_1}{\partial y^2}\right) + \left(-F_{55}\frac{\partial^2 w_2}{\partial x^2} + 4D_{33}w_2 - F_{44}\frac{\partial^2 w_2}{\partial y^2}\right)$$
$$+ (2D_{13} - D_{55})\frac{\partial u_1}{\partial x} + (2F_{13} - 3F_{55})\frac{\partial u_3}{\partial x} + (2D_{23} - D_{44})\frac{\partial v_1}{\partial y}$$
$$+ (2F_{23} - 3F_{44})\frac{\partial v_3}{\partial y} - \left(D_{55}\frac{\partial^2 w_0}{\partial x^2} + D_{44}\frac{\partial^2 w_0}{\partial y^2}\right) + 2B_{13}\frac{\partial u_0}{\partial x} + 2B_{23}\frac{\partial v_0}{\partial y}$$
$$= I_2\frac{\partial^2 w_0}{\partial t^2} + I_3\frac{\partial^2 w_1}{\partial t^2} + I_4\frac{\partial^2 w_2}{\partial t^2} + \left(\frac{h}{2}\right)^2 p_z \tag{50}$$

Being NL the number of mathematical layers across the thickness direction, the stiffness components can be computed as follows.

$$A_{ij} = \sum_{k=1}^{NL} c_{ij}^{(k)}\left(z_{k+1} - z_k\right); \qquad B_{ij} = \frac{1}{2}\sum_{k=1}^{NL} c_{ij}^{(k)}\left(z_{k+1}^2 - z_k^2\right) \tag{51}$$

$$D_{ij} = \frac{1}{3}\sum_{k=1}^{NL} c_{ij}^{(k)}\left(z_{k+1}^3 - z_k^3\right); \qquad E_{ij} = \frac{1}{4}\sum_{k=1}^{NL} c_{ij}^{(k)}\left(z_{k+1}^4 - z_k^4\right) \tag{52}$$

$$F_{ij} = \frac{1}{5}\sum_{k=1}^{NL} c_{ij}^{(k)}\left(z_{k+1}^5 - z_k^5\right); \qquad G_{ij} = \frac{1}{7}\sum_{k=1}^{NL} c_{ij}^{(k)}\left(z_{k+1}^7 - z_k^7\right) \tag{53}$$

The inertia terms are defined by

$$I_i = \frac{1}{i+1}\sum_{k=1}^{NL} \rho^{(k)}\left(z_{k+1}^{i+1} - z_k^{i+1}\right) \tag{54}$$

where $\rho^{(k)}$ is the material density, h_k is the thickness, and z_k, z_{k+1} are the lower and upper z coordinate for each layer k.

4.2 Natural boundary conditions

This meshless method based on collocation with radial basis functions needs the imposition of essential (e.g. $w = 0$) and mechanical (e.g. $M_{xx} = 0$) bound-

ary conditions. Assuming a rectangular plate (for the sake of simplicity) equations (29) are expressed as follows.

Given the number of degrees of freedom, at each boundary point at edges $x = min$ or $x = max$ we impose:

$$M_{xxu0} = 2B_{13}w_2 + A_{13}w_1 + A_{11}\frac{\partial u_0}{\partial x} + A_{12}\frac{\partial v_0}{\partial y} + B_{11}\frac{\partial u_1}{\partial x} + E_{11}\frac{\partial u_3}{\partial x} + B_{12}\frac{\partial v_1}{\partial y} + E_{12}\frac{\partial v_3}{\partial y} \quad (55)$$

$$M_{xxu1} = B_{13}w_1 + 2D_{13}w_2 + B_{11}\frac{\partial u_0}{\partial x} + D_{11}\frac{\partial u_1}{\partial x} + F_{11}\frac{\partial u_3}{\partial x} + B_{12}\frac{\partial v_0}{\partial y} + D_{12}\frac{\partial v_1}{\partial y} + F_{12}\frac{\partial v_3}{\partial y} \quad (56)$$

$$M_{xxu3} = E_{13}w_1 + 2F_{13}w_2 + E_{11}\frac{\partial u_0}{\partial x} + F_{11}\frac{\partial u_1}{\partial x} + G_{11}\frac{\partial u_3}{\partial x} + E_{12}\frac{\partial v_0}{\partial y} + F_{12}\frac{\partial v_1}{\partial y} + G_{12}\frac{\partial v_3}{\partial y} \quad (57)$$

$$M_{xxv0} = A_{66}\frac{\partial u_0}{\partial y} + A_{66}\frac{\partial v_0}{\partial x} + B_{66}\frac{\partial u_1}{\partial y} + E_{66}\frac{\partial u_3}{\partial y} + B_{66}\frac{\partial v_1}{\partial x} + E_{66}\frac{\partial v_3}{\partial x} \quad (58)$$

$$M_{xxv1} = B_{66}\frac{\partial u_0}{\partial y} + D_{66}\frac{\partial u_1}{\partial y} + F_{66}\frac{\partial u_3}{\partial y} + B_{66}\frac{\partial v_0}{\partial x} + D_{66}\frac{\partial v_1}{\partial x} + F_{66}\frac{\partial v_3}{\partial x} \quad (59)$$

$$M_{xxv3} = E_{66}\frac{\partial u_0}{\partial y} + F_{66}\frac{\partial u_1}{\partial y} + G_{66}\frac{\partial u_3}{\partial y} + E_{66}\frac{\partial v_0}{\partial x} + F_{66}\frac{\partial v_1}{\partial x} + G_{66}\frac{\partial v_3}{\partial x} \quad (60)$$

$$M_{xxw0} = 3D_{55}u_3 + A_{55}u_1 + A_{55}\frac{\partial w_0}{\partial x} + B_{55}\frac{\partial w_1}{\partial x} + D_{55}\frac{\partial w_2}{\partial x} \quad (61)$$

$$M_{xxw1} = B_{55}u_1 + 3E_{55}u_3 + B_{55}\frac{\partial w_0}{\partial x} + D_{55}\frac{\partial w_1}{\partial x} + E_{55}\frac{\partial w_2}{\partial x} \quad (62)$$

$$M_{xxw2} = D_{55}u_1 + 3F_{55}u_3 + D_{55}\frac{\partial w_0}{\partial x} + E_{55}\frac{\partial w_1}{\partial x} + F_{55}\frac{\partial w_2}{\partial x} \quad (63)$$

Similarly, given the number of degrees of freedom, at each boundary point at edges $y = min$ or $y = max$ we impose:

$$M_{yyu0} = A_{66}\frac{\partial u_0}{\partial y} + A_{66}\frac{\partial v_0}{\partial x} + B_{66}\frac{\partial u_1}{\partial y} + E_{66}\frac{\partial u_3}{\partial y} + B_{66}\frac{\partial v_1}{\partial x} + E_{66}\frac{\partial v_3}{\partial x} \quad (64)$$

$$M_{yyu1} = B_{66}\frac{\partial u_0}{\partial y} + D_{66}\frac{\partial u_1}{\partial y} + F_{66}\frac{\partial u_3}{\partial y} + B_{66}\frac{\partial v_0}{\partial x} + D_{66}\frac{\partial v_1}{\partial x} + F_{66}\frac{\partial v_3}{\partial x} \quad (65)$$

$$M_{yyu3} = E_{66}\frac{\partial u_0}{\partial y} + F_{66}\frac{\partial u_1}{\partial y} + G_{66}\frac{\partial u_3}{\partial y} + E_{66}\frac{\partial v_0}{\partial x} + F_{66}\frac{\partial v_1}{\partial x} + G_{66}\frac{\partial v_3}{\partial x} \quad (66)$$

$$M_{yyv0} = A_{12}\frac{\partial u_0}{\partial x} + A_{22}\frac{\partial v_0}{\partial y} + B_{12}\frac{\partial u_1}{\partial x} + E_{12}\frac{\partial u_3}{\partial x} + B_{22}\frac{\partial v_1}{\partial y} + E_{22}\frac{\partial v_3}{\partial y} \quad (67)$$

$$M_{yyv1} = B_{12}\frac{\partial u_0}{\partial x} + D_{12}\frac{\partial u_1}{\partial x} + F_{12}\frac{\partial u_3}{\partial x} + B_{22}\frac{\partial v_0}{\partial y} + D_{22}\frac{\partial v_1}{\partial y} + F_{22}\frac{\partial v_3}{\partial y} \quad (68)$$

$$M_{yyv3} = E_{12}\frac{\partial u_0}{\partial x} + F_{12}\frac{\partial u_1}{\partial x} + G_{12}\frac{\partial u_3}{\partial x} + E_{22}\frac{\partial v_0}{\partial y} + F_{22}\frac{\partial v_1}{\partial y} + G_{22}\frac{\partial v_3}{\partial y} \quad (69)$$

$$M_{yyw0} = 3D_{44}v_3 + A_{44}v_1 + A_{44}\frac{\partial w_0}{\partial y} + B_{44}\frac{\partial w_1}{\partial y} + D_{44}\frac{\partial w_2}{\partial y} \quad (70)$$

$$M_{yyw1} = B_{44}v_1 + 3E_{44}v_3 + B_{44}\frac{\partial w_0}{\partial y} + D_{44}\frac{\partial w_1}{\partial y} + E_{44}\frac{\partial w_2}{\partial y} \quad (71)$$

$$M_{yyw2} = D_{44}v_1 + 3F_{44}v_3 + D_{44}\frac{\partial w_0}{\partial y} + E_{44}\frac{\partial w_1}{\partial y} + F_{44}\frac{\partial w_2}{\partial y} \quad (72)$$

with A_{ij}, B_{ij}, D_{ij}, E_{ij}, F_{ij}, G_{ij} as in (53).

5 The radial basis function method

The governing equations are interpolated by radial basis function method. This meshless method was first used by Hardy [65] in the early 1970's for the interpolation of geographical data. Kansa [66] introduced in 1990 the concept of solving partial differential equations (PDE) by an unsymmetric RBF collocation method based upon the multiquadric interpolation functions. For the sake of completeness we present in the following the basics of collocation with radial basis functions for static, vibrations, and buckling problems.

5.1 The static problem

In this section the formulation of a global unsymmetrical collocation RBF-based method to compute elliptic operators is presented. Consider a linear elliptic partial differential operator $\mathcal{L}$ and a bounded region Ω in $\mathbb{R}^n$ with some boundary $\partial\Omega$. In the static problems we seek the computation of displacements ($\mathbf{u}$) from the global system of equations

$$\mathcal{L}\mathbf{u} = \mathbf{f} \text{ in } \Omega; \qquad \mathcal{L}_B\mathbf{u} = \mathbf{g} \text{ on } \partial\Omega \tag{73}$$

where $\mathcal{L}$, $\mathcal{L}_B$ are linear operators in the domain and on the boundary, respectively. The right-hand sides in (73) represent the external forces applied on the plate and the boundary conditions applied along the perimeter of the plate, respectively. The PDE problem defined in (73) will be replaced by a finite problem, defined by an algebraic system of equations, after the radial basis expansions.

5.2 The eigenproblem

The eigenproblem looks for eigenvalues (λ) and eigenvectors ($\mathbf{u}$) that satisfy

$$\mathcal{L}\mathbf{u} + \lambda\mathbf{u} = 0 \text{ in } \Omega; \qquad \mathcal{L}_B\mathbf{u} = 0 \text{ on } \partial\Omega \tag{74}$$

As in the static problem, the eigenproblem defined in (74) is replaced by a finite-dimensional eigenvalue problem, based on RBF approximations.

5.3 Radial basis functions approximations

The radial basis function (ϕ) approximation of a function ($\mathbf{u}$) is given by

$$\tilde{\mathbf{u}}(\mathbf{x}) = \sum_{i=1}^{N} \alpha_i \phi\left(\|x - y_i\|_2\right), \mathbf{x} \in \mathbb{R}^n \tag{75}$$

where $y_i, i = 1, .., N$ is a finite set of distinct points (centers) in $\mathbb{R}^n$. Examples of the many RBFs that can be used are

$$\phi(r) = r^3, \qquad \text{cubic} \tag{76}$$
$$\phi(r) = e^{-(cr)^2}, \qquad \text{Gaussian} \tag{77}$$
$$\phi(r) = \sqrt{c^2 + r^2}, \qquad \text{Multiquadric} \tag{78}$$

where the Euclidean distance r is real and non-negative and c is a positive user defined shape parameter.

Considering N distinct interpolations, and knowing $u(x_j), j = 1, 2, ..., N$, we find α_i by the solution of a $N \times N$ linear system

$$\mathbf{A}\boldsymbol{\alpha} = \mathbf{u} \tag{79}$$

where $\mathbf{A} = \left[\phi\left(\|x - y_i\|_2\right)\right]_{N\times N}$, $\boldsymbol{\alpha} = [\alpha_1, \alpha_2, ..., \alpha_N]^T$ and $\mathbf{u} = [u(x_1), u(x_2), ..., u(x_N)]^T$.

5.4 Solution of the static problem

The solution of a static problem by radial basis functions considers N_I nodes in the domain and N_B nodes on the boundary, with a total number of nodes $N = N_I + N_B$. We denote the sampling points by $x_i \in \Omega, i = 1, ..., N_I$ and $x_i \in \partial\Omega, i = N_I + 1, ..., N$. At the points in the domain we solve the following system of equations

$$\sum_{i=1}^{N} \alpha_i \mathcal{L}\phi\left(\|x - y_i\|_2\right) = \mathbf{f}(x_j), j = 1, 2, ..., N_I \tag{80}$$

or

$$\mathcal{L}^I \boldsymbol{\alpha} = \mathbf{F} \tag{81}$$

where

$$\mathcal{L}^I = \left[\mathcal{L}\phi\left(\|x - y_i\|_2\right)\right]_{N_I\times N} \tag{82}$$

At the points on the boundary, we impose boundary conditions as

$$\sum_{i=1}^{N} \alpha_i \mathcal{L}_B \phi \left(\|x - y_i\|_2 \right) = \mathbf{g}(x_j), j = N_I + 1, ..., N \tag{83}$$

or

$$\mathbf{B}\boldsymbol{\alpha} = \mathbf{G} \tag{84}$$

where

$$\mathbf{B} = \mathcal{L}_B \phi \left[(\|x_{N_I+1} - y_j\|_2) \right]_{N_B \times N}$$

Therefore, we can write a finite-dimensional static problem as

$$\begin{bmatrix} \mathcal{L}^I \\ \mathbf{B} \end{bmatrix} \boldsymbol{\alpha} = \begin{bmatrix} \mathbf{F} \\ \mathbf{G} \end{bmatrix} \tag{85}$$

By inverting the system (85), we obtain the vector $\boldsymbol{\alpha}$. We then obtain the solution $\mathbf{u}$ using the interpolation equation (75).

5.5 Solution of the eigenproblem

We consider N_I nodes in the interior of the domain and N_B nodes on the boundary, with $N = N_I + N_B$. We denote interpolation points by $x_i \in \Omega, i = 1, ..., N_I$ and $x_i \in \partial\Omega, i = N_I + 1, ..., N$. At the points in the domain, we define the eigenproblem as

$$\sum_{i=1}^{N} \alpha_i \mathcal{L} \phi \left(\|x - y_i\|_2 \right) = \lambda \tilde{\mathbf{u}}(x_j), j = 1, 2, ..., N_I \tag{86}$$

or

$$\mathcal{L}^I \boldsymbol{\alpha} = \lambda \tilde{\mathbf{u}}^I \tag{87}$$

where

$$\mathcal{L}^I = \left[\mathcal{L} \phi \left(\|x - y_i\|_2 \right) \right]_{N_I \times N} \tag{88}$$

At the points on the boundary, we enforce the boundary conditions as

$$\sum_{i=1}^{N} \alpha_i \mathcal{L}_B \phi \left(\|x - y_i\|_2 \right) = 0, j = N_I + 1, ..., N \tag{89}$$

or

$$\mathbf{B}\boldsymbol{\alpha} = 0 \tag{90}$$

Equations (87) and (90) can now be solved as a generalized eigenvalue problem

$$\begin{bmatrix} \mathcal{L}^I \\ \mathbf{B} \end{bmatrix} \boldsymbol{\alpha} = \lambda \begin{bmatrix} \mathbf{A}^I \\ \mathbf{0} \end{bmatrix} \boldsymbol{\alpha} \tag{91}$$

where

$$\mathbf{A}^I = \phi \left[(\|x_{N_I} - y_j\|_2) \right]_{N_I \times N}$$

5.6 Discretization of the governing equations and boundary conditions

The radial basis collocation method follows a simple implementation procedure. Taking equation (85), we compute

$$\boldsymbol{\alpha} = \begin{bmatrix} L^I \\ \mathbf{B} \end{bmatrix}^{-1} \begin{bmatrix} \mathbf{F} \\ \mathbf{G} \end{bmatrix} \tag{92}$$

This $\boldsymbol{\alpha}$ vector is then used to obtain solution $\tilde{\mathbf{u}}$, by using (75). If derivatives of $\tilde{\mathbf{u}}$ are needed, such derivatives are computed as

$$\frac{\partial \tilde{\mathbf{u}}}{\partial x} = \sum_{j=1}^{N} \alpha_j \frac{\partial \phi_j}{\partial x}; \qquad \frac{\partial^2 \tilde{\mathbf{u}}}{\partial x^2} = \sum_{j=1}^{N} \alpha_j \frac{\partial^2 \phi_j}{\partial x^2}, \text{etc} \tag{93}$$

In the present collocation approach, we need to impose essential and natural boundary conditions. Consider, for example, the condition $w_0 = 0$, on a simply supported or clamped edge. We enforce the conditions by interpolating as

$$w_0 = 0 \rightarrow \sum_{j=1}^{N} \alpha_j^{W_0} \phi_j = 0 \tag{94}$$

Other boundary conditions are interpolated in a similar way.

5.7 Free vibrations problems

For free vibration problems we set the external force to zero, and assume harmonic solution in terms of displacements $u_0, u_1, u_3, v_0, v_1, v_3, w_0, w_1, w_2$ as

$$
\begin{aligned}
&u_0 = U_0(w,y)e^{i\omega t}; \quad u_1 = U_1(w,y)e^{i\omega t}; \quad u_3 = U_3(w,y)e^{i\omega t};\\
&v_0 = V_0(w,y)e^{i\omega t}; \quad v_1 = V_1(w,y)e^{i\omega t}; \quad v_3 = V_3(w,y)e^{i\omega t};\\
&w_0 = W_0(w,y)e^{i\omega t}; \quad w_1 = W_1(w,y)e^{i\omega t}; \quad w_2 = W_2(w,y)e^{i\omega t}
\end{aligned} \tag{95}
$$

where ω is the frequency of natural vibration. Substituting the harmonic expansion into equations (91) in terms of the amplitudes $U_0, U_1, U_3,\ V_0, V_1, V_3,\ W_0, W_1, W_2$, we may obtain the natural frequencies and vibration modes for the plate problem, by solving the eigenproblem

$$
\left[\mathcal{L} - \omega^2 \mathcal{G}\right] \mathbf{X} = \mathbf{0} \tag{96}
$$

where $\mathcal{L}$ collects all stiffness terms and $\mathcal{G}$ collects all terms related to the inertial terms. In (96) $\mathbf{X}$ are the modes of vibration associated with the natural frequencies defined as ω.

5.8 Buckling problems

The eigenproblem associated to the governing equations is defined as

$$
\left[\mathcal{L} - \lambda \mathcal{G}\right] \mathbf{X} = \mathbf{0} \tag{97}
$$

where $\mathcal{L}$ collects all stiffness terms and $\mathcal{G}$ collects all terms related to the in-plane forces. In (97) $\mathbf{X}$ are the buckling modes associated with the buckling loads defined as λ.

6 Numerical examples

In the next examples the higher-order plate theory presented before and collocation with RBFs are used for the analysis of simply supported functionally graded square plates. For the $\epsilon_{zz} = 0$ case, we consider $w = w_0$ instead of (7).

All examples use the Wendland RBF function [67] defined as

$$
\phi(r) = (1 - cr)_+^8 \left(32(cr)^3 + 25(cr)^2 + 8cr + 1\right) \tag{98}
$$

The shape parameter (c) is obtained by an optimization procedure as detailed in Ferreira and Fasshauer [68]. The interpolation points are Chebyshev

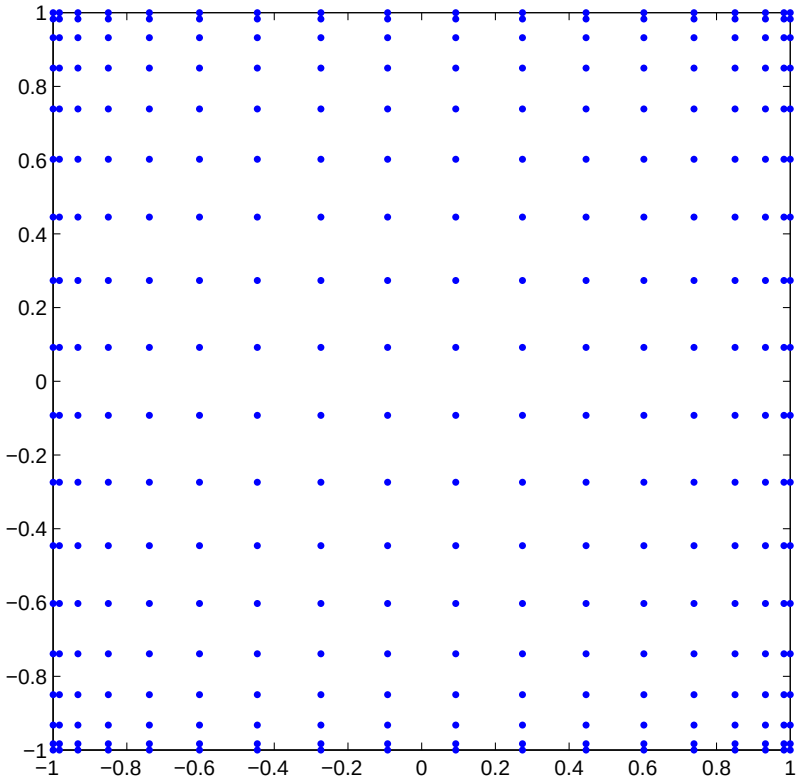

Fig. 6. Chebyshev grid with N=17

$\mathbb{R}^2$ points. For a given number of nodes per side (N) they are generated by MATLAB code as:

```
x = cos(pi*(0:N)/N)'; y=x;
```

A 17^2 points Chebyshev grid is illustrated in figure 6.

91 mathematical layers were considered in order to model the continuous variation of properties across the thickness direction. A significant number of mathematical layers is needed to ensure correct computation of material properties at each thickness position. The Young's modulus of each layer, $E^k(z)$, are computed considering a simple law-of-mixtures (33) or the Mori-Tanaka procedure (36). Poisson's ratio is considered constant for both materials $\nu_m = \nu_c = \nu = 0.3$.

grid	13^2	17^2	21^2
w	0.5868	0.5868	0.5868

Table 1
w convergence study for the bending analysis of plate A using higher-order plate theory, $p = 1$, and $a/h = 10$.

grid	13^2	17^2	21^2
σ_{xx}	1.4911	1.4917	1.4917

Table 2
σ_{xx} convergence study for the bending analysis of plate A using higher-order plate theory, $p = 1$, and $a/h = 10$.

6.1 Plates on bending

The plate is subjected to a bi-sinusoidal transverse mechanical load of amplitude load $p_z = \bar{p}_z sin\left(\frac{\pi x}{a}\right) sin\left(\frac{\pi y}{a}\right)$ applied at the top of the plate with $\bar{p}_z = 1$. It is important to note that the load is applied at the top surface ($z = h/2$), which is not only physically correct as it makes all the difference in terms of the displacement and stresses evolution. The right-hand side of the governing equations given in section 4.1 and the terms including the in-plane forces are zero.

6.1.1 Isotropic FGM square plate

In this example, an isotropic FGM square plate of type A is considered. The plate is graded from aluminum $E_m = 70$ GPa at the bottom to alumina $E_c = 380$ GPa at the top. The law-of-mixtures was used for the Young's modulus.

The in-plane displacements, the transverse displacements, the normal stresses and the in-plane and transverse shear stresses are presented in normalized form as

$$\bar{u}_z = \frac{10h^3 E_c}{a^4 \bar{p}_z} u_z, \quad \bar{\sigma}_{xx} = \frac{h}{a\bar{p}_z}\sigma_{xx}, \quad \bar{\sigma}_{xz} = \frac{h}{a\bar{p}_z}\sigma_{xz}, \quad \bar{\sigma}_{zz} = \sigma_{zz} \tag{99}$$

An initial convergence study was performed for $\sigma_{xx}\left(\frac{h}{3}\right)$ and transverse displacement $w(0)$ at the center of the plate, considering $p = 1$, $a/h = 10$, and Chebyshev grids of 13^2, 17^2, and 21^2 points. Results are presented in tables 1 and 2.

In table 3 we present results for σ_{xx} and transverse displacement for various

exponents p of the power-law (2) considering a 17^2 points grid. The considered side-to-thickness ratios a/h are 4, 10 and 100, which means thickness h equals 0.25, 0.1 and 0.01, respectively. Results are compared with the Classical Plate Theory (CLPT), the first-order shear deformation theory (FSDT) with a correction factor $k = 5/6$, and those from Zenkour's generalized shear deformation theory [19], considering $\epsilon_{zz} = 0$, and those from Carrera et al. [46,47], and Neves et al. [61], accounting for ϵ_{zz}.

The results from present higher-order plate theory considering $\epsilon_{zz} \neq 0$ are in good agreement with those from references [46,47] and [61] who also considers $\epsilon_{zz} \neq 0$. The present theory allows to conclude that the values of σ_{xx} and transverse displacement considering $\epsilon_{zz} = 0$ are higher than those considering $\epsilon_{zz} \neq 0$. These differences decrease as the thickness of the plate decreases which is not surprising as thicker plates can stretch more in the thickness direction.

In figures 7 and 8 we present the evolution of the displacement and stresses across the thickness direction according to present shear deformation theory for various values of the exponent p, and side to thickness ratio $a/h = 4$, using a 19^2 grid.

6.1.2 Sandwich with FGM core

In this example we analyse the bending of a square sandwich plate of type B with thickness h. The bottom skin is aluminium ($E_m = 70$ GPa) with thickness $h_b = 0.1h$ and the top skin is alumina ($E_c = 380$ GPa) with thickness $h_t = 0.1h$. The core is in FGM with volume fraction of the ceramic according to (3). The functional relationship for YoungŠs modulus $E^k(z)$ in the thickness direction z is obtained from the rule of mixtures as in (33).

The transverse displacement and the normal stresses are presented in normalized form as

$$\begin{aligned} \bar{u}_z &= \frac{10h^3 E_c}{a^4 \bar{p}_z} u_z\left(\frac{a}{2}, \frac{b}{2}\right), \quad \bar{\sigma}_{xx} = \frac{h}{a\bar{p}_z}\sigma_{xx}\left(\frac{a}{2}, \frac{b}{2}\right) \\ \bar{\sigma}_{yy} &= \frac{h}{a\bar{p}_z}\sigma_{yy}\left(\frac{a}{2}, \frac{b}{2}\right), \quad \bar{\sigma}_{zz} = \sigma_{zz}\left(\frac{a}{2}, \frac{b}{2}\right) \end{aligned} \tag{100}$$

The transverse shear stresses are normalized according to

$$\bar{\sigma}_{xy} = \frac{h}{a\bar{p}_z}\sigma_{xy}\left(0, 0\right), \quad \bar{\sigma}_{xz} = \frac{h}{a\bar{p}_z}\sigma_{xz}\left(0, \frac{b}{2}\right), \quad \bar{\sigma}_{yz} = \frac{h}{a\bar{p}_z}\sigma_{yz}\left(\frac{a}{2}, 0\right) \tag{101}$$

p		ϵ_{zz}	$\bar{\sigma}_{xx}(h/3)$			$\bar{u}_z(0)$		
	a/h		4	10	100	4	10	100
1	Ref. [46]	$\neq 0$	0.6221	1.5064	14.969	0.7171	0.5875	0.5625
	CLPT	0	0.8060	2.0150	20.150	0.5623	0.5623	0.5623
	FSDT(k=5/6)	0	0.8060	2.0150	20.150	0.7291	0.5889	0.5625
	GSDT [19]	0		1.4894			0.5889	
	Ref. [47] N=4	0	0.7856	2.0068	20.149	0.7289	0.5890	0.5625
	Ref. [47] N=4	$\neq 0$	0.6221	1.5064	14.969	0.7171	0.5875	0.5625
	Ref. [61]	$\neq 0$	0.5925	1.4945	14.969	0.6997	0.5845	0.5624
	Present	0	0.5806	1.4874	14.944	0.7308	0.5913	0.5648
	Present	$\neq 0$	0.5911	1.4917	14.945	0.7020	0.5868	0.5647
4	Ref. [46]	$\neq 0$	0.4877	1.1971	11.923	1.1585	0.8821	0.8286
	CLPT	0	0.6420	1.6049	16.049	0.8281	0.8281	0.8281
	FSDT(k=5/6)	0	0.6420	1.6049	16.049	1.1125	0.8736	0.828
	GSDT [19]	0		1.1783			0.8651	
	Ref. [47] N=4	0	0.5986	1.5874	16.047	1.1673	0.8828	0.8286
	Ref. [47] N=4	$\neq 0$	0.4877	1.1971	11.923	1.1585	0.8821	0.8286
	Ref. [61]	$\neq 0$	0.4404	1.1783	11.932	1.1178	0.8750	0.8286
	Present	0	0.4338	1.1592	11.737	1.1552	0.8770	0.8241
	Present	$\neq 0$	0.4330	1.1588	11.737	1.1108	0.8700	0.8240
10	Ref. [46]	$\neq 0$	0.3695	0.8965	8.9077	1.3745	1.0072	0.9361
	CLPT	0	0.4796	1.1990	11.990	0.9354	0.9354	0.9354
	FSDT(k=5/6)	0	0.4796	1.1990	11.990	1.3178	0.9966	0.9360
	GSDT [19]	0		0.8775			1.0089	
	Ref. [47] N=4	0	0.4345	1.1807	11.989	1.3925	1.0090	0.9361
	Ref. [47] N=4	$\neq 0$	0.1478	0.8965	8.9077	1.3745	1.0072	0.9361
	Ref. [61]	$\neq 0$	0.3227	1.1783	11.932	1.3490	0.8750	0.8286
	Present	0	0.3112	0.8468	8.6011	1.3760	0.9952	0.9228
	Present	$\neq 0$	0.3097	0.8462	8.6010	1.3334	0.9888	0.9227

Table 3
FGM isotropic plate type A on bending. Effect of transverse normal strain ϵ_{zz} on σ_{xx} and deflection under present higher-order theory and using 17^2 points.

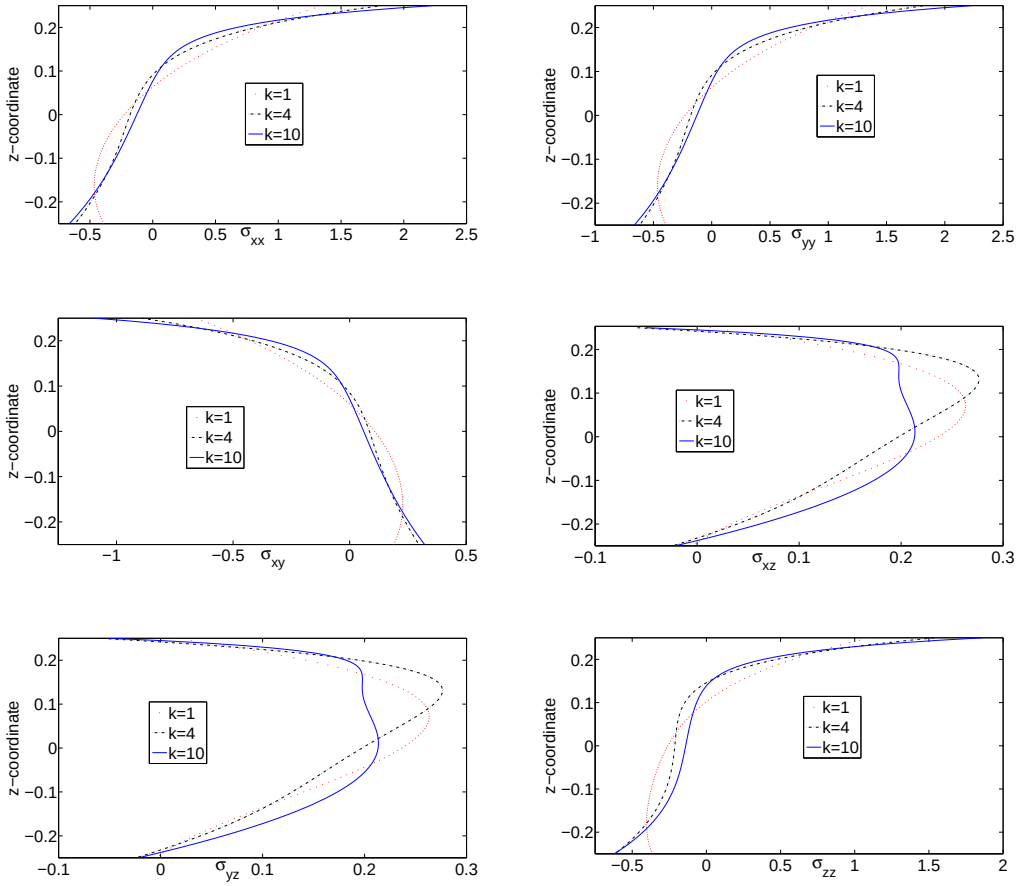

Fig. 7. FGM square plate subjected to sinusoidal load at the top, with $a/h = 4$. Stresses through the thickness direction according to present higher-order theory for different values of p.

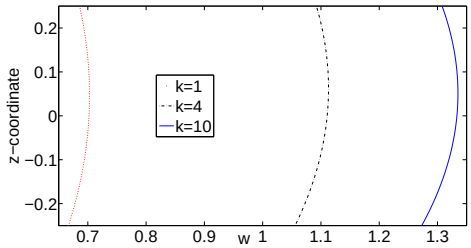

Fig. 8. FGM square plate subjected to sinusoidal load at the top, with $a/h = 4$. Displacement through the thickness direction according to present higher-order theory for different values of p.

An initial convergence study was performed for $\sigma_{xz}\left(\frac{h}{6}\right)$ and transverse displacement $w(0)$ considering $p = 4$, $a/h = 100$, and Chebyshev grids of 13^2, 17^2, 19^2, and 21^2 points. Results are presented in tables 4 and 5.

In table 6 we present the values of σ_{xz} and out-of-plane displacement for

grid	13^2	17^2	19^2	21^2
w	0.7749	0.7782	0.7784	0.7785

Table 4
w convergence study for the bending analysis of plate B using higher-order plate theory, $p = 4$, and $a/h = 100$.

grid	13^2	17^2	19^2	21^2
σ_{xz}	0.2696	0.2749	0.2753	0.2753

Table 5
σ_{xz} convergence study for the bending analysis of plate B using higher-order plate theory, $p = 4$, and $a/h = 100$.

various values of exponent p of the material power-law ($p = 1, 4, 10$) and various thickness to side ratios ($a/h = 4, 10, 100$) according to the present higher-order theory considering zero and non-zero ϵ_{zz} strain using 19^2 points. Results are tabulated and compared with available references.

In figures 9 and 10 we present the evolution of the displacement and stresses across the thickness direction according to present shear deformation theory for various values of the exponent p of a plate with side to thickness ratio $a/h = 100$, using a 19^2 grid.

6.2 Free vibration of plates

For the vibration analysis it is assumed that there are no external forces applied in the plate. In this example we study the free vibration of a simply supported isotropic FGM square plate ($a = b = 1$) of type A. The plate is graded from aluminum (bottom) to zirconia (top). $E_m = 70$ GPa and $E_c = 200$ GPa are the corresponding properties of the metal and zirconia, respectively.

We consider the Mori-Tanaka homogeneization scheme (36), the same used in the literature we use as a reference: the exact solution by Vel and Batra [69], and the one obtained with a meshless technique by Qian et al. [70].

The frequency w has been non-dimensionalized as follows:

$$\bar{w} = wh\sqrt{\rho_m/E_m} \tag{102}$$

In table 7 we present the results obtained with the theories considered and different values of p for a side to thickness ratio $a/h = 5$.

The first 10 natural frequencies obtained with present higher-order shear deformation theorie are listed in tables 8 ($a/h = 20$) and 9 ($a/h = 10$) for $p = 1$

p		ϵ_{zz}	$\bar{\sigma}_{xz}(h/6)$			$\bar{u}_z(0)$		
	a/h		4	10	100	4	10	100
1	Ref. [45]	$\neq 0$	0.2613	0.2605	0.2603	0.7628	0.6324	0.6072
	CLPT	0	0.0000	0.0000	0.0000	0.6070	0.6070	0.6070
	FSDT(k=5/6)	0	0.2458	0.2458	0.2458	0.7738	0.6337	0.6073
	Ref. [47] N=4	0	0.2596	0.2593	0.2593	0.7735	0.6337	0.6072
	Ref. [47] N=4	$\neq 0$	0.2604	0.2594	0.2593	0.7628	0.6324	0.6072
	Ref. [61]	0	0.2703	0.2718	0.2720	0.7744	0.6356	0.6092
	Ref. [61]	$\neq 0$	0.2742	0.2788	0.2793	0.7416	0.6305	0.6092
	Present	0	0.2706	0.2720	0.2721	0.7746	0.6357	0.6092
	Present	$\neq 0$	0.2745	0.2789	0.2795	0.7417	0.6305	0.6092
4	Ref. [45]	$\neq 0$	0.2429	0.2431	0.2432	1.0934	0.8321	0.7797
	CLPT	0	0.0000	0.0000	0.0000	0.7792	0.7792	0.7792
	FSDT(k=5/6)	0	0.1877	0.1877	0.1877	1.0285	0.8191	0.7796
	Ref. [47] N=4	0	0.2400	0.2398	0.2398	1.0977	0.8308	0.7797
	Ref. [47] N=4	$\neq 0$	0.2400	0.2398	0.2398	1.0930	0.8307	0.7797
	Ref. [61]	0	0.2699	0.2726	0.2728	1.0847	0.8276	0.7785
	Ref. [61]	$\neq 0$	0.2723	0.2778	0.2785	1.0391	0.8202	0.7784
	Present	0	0.2671	0.2695	0.2696	1.0826	0.8272	0.7785
	Present	$\neq 0$	0.2696	0.2747	0.2753	1.0371	0.8199	0.7784
10	Ref. [45]	$\neq 0$	0.2150	0.2174	0.2179	1.2232	0.8753	0.8077
	CLPT	0	0.0000	0.0000	0.0000	0.8070	0.8070	0.8070
	FSDT(k=5/6)	0	0.1234	0.1234	0.1234	1.1109	0.8556	0.8075
	Ref. [47] N=4	0	0.1935	0.1944	0.1946	1.2240	0.8743	0.8077
	Ref. [47] N=4	$\neq 0$	0.1932	0.1944	0.1946	1.2172	0.8740	0.8077
	Ref. [61]	0	0.1998	0.2021	0.2022	1.2212	0.8718	0.8050
	Ref. [61]	$\neq 0$	0.2016	0.2059	0.2064	1.1780	0.8650	0.8050
	Present	0	0.1996	0.2018	0.2019	1.2183	0.8712	0.8050
	Present	$\neq 0$	0.1995	0.2034	0.2039	1.1752	0.8645	0.8050

Table 6
Sandwich square plate with FGM core type B on bending. Effect of transverse normal strain ϵ_{zz} on σ_{xz} and w according to present higher-order plate theory, using 19^2 points.

source	$p=1$	$p=2$	$p=3$	$p=5$
Exact [69]	0.2192	0.2197	0.2211	0.2225
Ref. [70]	0.2152	0.2153	0.2172	0.2194
Ref. [61] ($\epsilon_{zz}=0$)	0.2184	0.2189	0.2202	0.2215
Ref. [61] ($\epsilon_{zz}\neq 0$)	0.2193	0.2198	0.2212	0.2225
Present ($\epsilon_{zz}=0$)	0.2184	0.2191	0.2206	0.2220
Present ($\epsilon_{zz}\neq 0$)	0.2193	0.2200	0.2215	0.2230

Table 7
Fundamental frequency of a SSSS isotropic functionally graded plate (Al/ZrO_2) square plate with $a/h=0.2$ using a 21^2 grid.

source	1	2	3	4	5	6	7	8	9	10
Ref. [70]	0.0149	0.0377	0.0377	0.0593	0.0747	0.0747	0.0769	0.0912	0.0913	0.1029
Ref. [61]	0.0153	0.0377	0.0377	0.0596	0.0739	0.0739	0.0950	0.0950	0.1029	0.1029
$\epsilon_z=0$ 13^2	0.0153	0.0377	0.0377	0.0596	0.0740	0.0740	0.0951	0.0951	0.1030	0.1030
$\epsilon_z\neq 0$ 13^2	0.0153	0.0377	0.0377	0.0596	0.0741	0.0741	0.0953	0.0953	0.1030	0.1030
$\epsilon_z=0$ 17^2	0.0153	0.0377	0.0377	0.0595	0.0738	0.0738	0.0949	0.0949	0.1030	0.1030
$\epsilon_z\neq 0$ 17^2	0.0153	0.0377	0.0377	0.0596	0.0739	0.0739	0.0950	0.0950	0.1030	0.1030
$\epsilon_z=0$ 21^2	0.0153	0.0377	0.0377	0.0595	0.0738	0.0738	0.0948	0.0948	0.1030	0.1030
$\epsilon_z\neq 0$ 21^2	0.0153	0.0377	0.0377	0.0596	0.0739	0.0739	0.0950	0.0950	0.1030	0.1030

Table 8
First 10 frequencies of a SSSS isotropic functionally graded plate (Al/ZrO_2) square plate with $p=1$ with $a/h=20$.

source	1	2	3	4	5	6	7	8	9	10
Ref. [70]	0.0584	0.1410	0.1410	0.2058	0.2058	0.2164	0.2646	0.2677	0.2913	0.3264
Ref. [61]	0.0596	0.1426	0.1426	0.2058	0.2058	0.2193	0.2676	0.2676	0.2910	0.3363
$\epsilon_z=0$ 13^2	0.0595	0.1422	0.1422	0.2059	0.2059	0.2185	0.2664	0.2664	0.2912	0.3347
$\epsilon_z\neq 0$ 13^2	0.0596	0.1426	0.1426	0.2059	0.2059	0.2194	0.2678	0.2678	0.2912	0.3367
$\epsilon_z=0$ 17^2	0.0595	0.1422	0.1422	0.2059	0.2059	0.2184	0.2663	0.2663	0.2912	0.3344
$\epsilon_z\neq 0$ 17^2	0.0596	0.1426	0.1426	0.2059	0.2059	0.2193	0.2676	0.2676	0.2912	0.3364
$\epsilon_z=0$ 21^2	0.0595	0.1422	0.1422	0.2059	0.2059	0.2184	0.2663	0.2663	0.2912	0.3344
$\epsilon_z\neq 0$ 21^2	0.0596	0.1426	0.1426	0.2059	0.2059	0.2193	0.2676	0.2676	0.2912	0.3364

Table 9
First 10 frequencies of a SSSS isotropic functionally graded plate (Al/ZrO_2) square plate with $p=1$ with $a/h=10$.

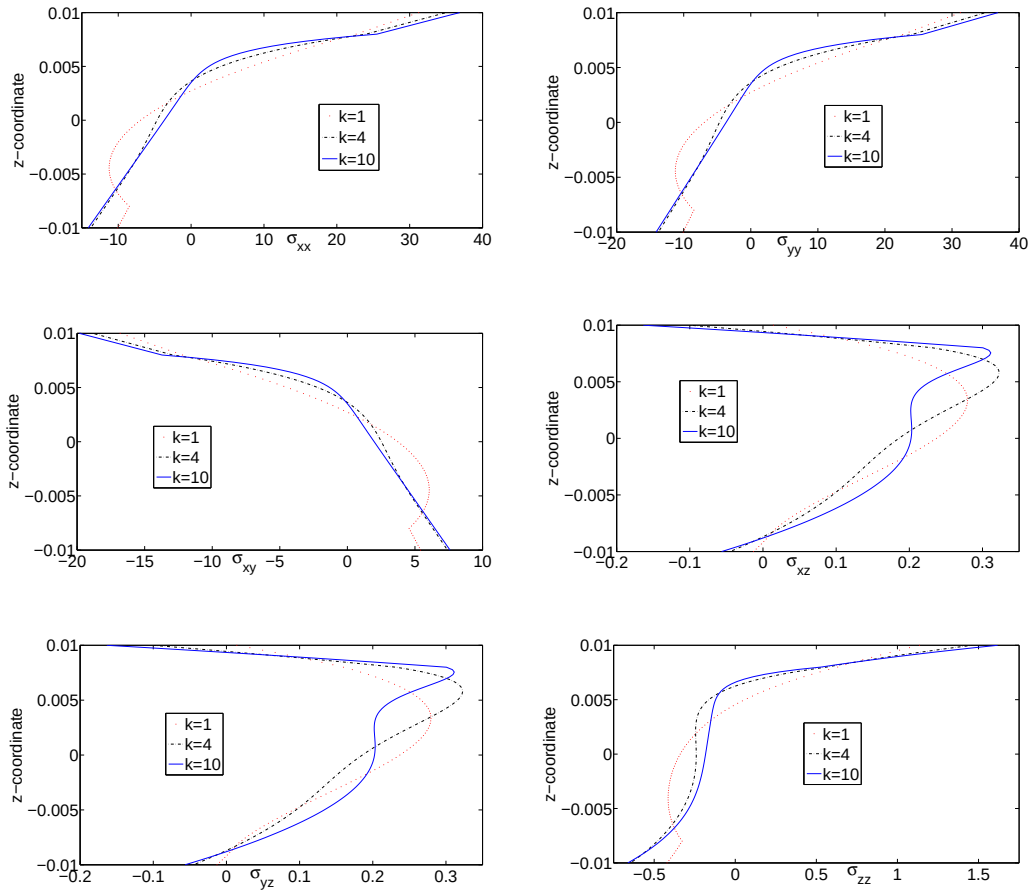

Fig. 9. Sandwich square plate with FGM core subjected to sinusoidal load at the top, with $a/h = 100$. Stresses through the thickness direction according to present higher-order theory for different values of p.

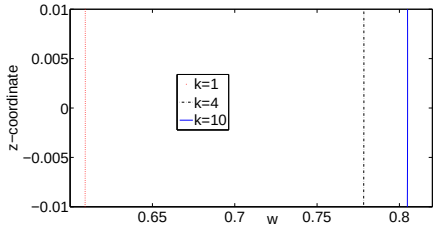

Fig. 10. Sandwich square plate with FGM core type B subjected to sinusoidal load at the top, with $a/h = 100$. Displacement through the thickness direction according to present higher-order theory for different values of p.

In figure 11 the first 4 frequencies of a simply supported isotropic functionally graded (Al/ZrO2) square plate, with $p = 1$, a 21^2 grid, using present higher-order shear deformation theory and a side to thickness ratio $a/h = 20$ are presented.

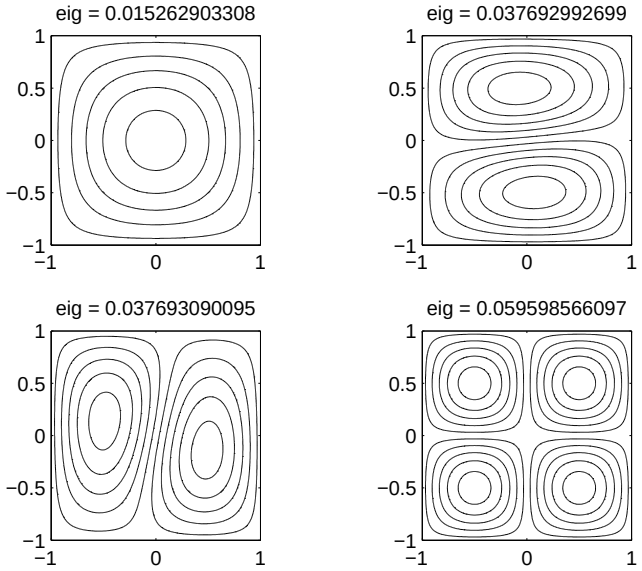

Fig. 11. First 4 frequencies of a SSSS isotropic functionally graded (Al/ZrO2) square plate, with $p = 1$, a 21^2 grid, present higher-order shear deformation theory and $a/h = 20$.

6.3 Buckling loads of plates

In the next examples the higher-order plate theory and collocation with RBFs are used for the buckling analysis of simply supported functionally graded sandwich square plates ($a = b$) of type C with side-to-thickness ratio $a/h = 10$. The uni- and bi-axial critical buckling loads are analised. For the buckling analysis we assume that all other mechanical loads are zero and the right-hand side of equations in section 4.1 are set to zero as well.

The material properties are $E_m = 70E_0$ (aluminum) for the metal and $E_c = 380E_0$ (alumina) for the ceramic being $E_0 = 1$GPa. The law-of-mixtures (33) was used for the Young's modulus. The non-dimensional parameter used is

$$\bar{P} = \frac{Pa^2}{100h^3E_0}.$$

An initial convergence study with the higher-order theory was conducted for each buckling load type considerind grids of 13^2, 17^2, and 21^2 points. The uni-axial case is presented in table 10 for the 2-2-1 sandwich with $p = 5$ and the bi-axial case is presented in table 11 for the 1-2-1 sandwich with $p = 1$. Further results are obtained by considering a grid of 17^2 points.

The critical buckling loads obtained from the present approach with $\epsilon_{zz} \neq 0$ and $\epsilon_{zz} = 0$ are tabulated and compared with those from Zenkour [29]

grid	13^2	17^2	21^2
$\bar{P}$	4.05112	4.05070	4.05065

Table 10
Convergence study for the uni-axial buckling load of a simply supported 2-2-1 sandwich square plate with FGM skins and $p = 5$ case using the higher-order theory.

grid	13^2	17^2	21^2
$\bar{P}$	3.66028	3.65998	3.65994

Table 11
Convergence study for the bi-axial buckling load of a simply supported 1-2-1 sandwich square plate with FGM skins and $p = 1$ case using the higher-order theory.

in tables 12 and 13 for various power-law exponents p and thickness ratios. Both tables include results obtained from classical plate theory (CLPT), first-order shear deformation plate theory (FSDPT, $K = 5/6$ as shear correction factor), Reddy's higher-order shear deformation plate theory (TSDPT) [10], and Zenkour's sinusoidal shear deformation plate theory (SSDPT) [29]. Table 12 refers to the uni-axial buckling load and table 13 refers to the bi-axial buckling load.

There is a good agreement between the present solution and references considered, specially [10] and [29]. This allow us to conclude that the present higher-order plate theory is good for the modeling of simply supported sandwich FGM plates and that collocation with RBFs is a good formulation. Present results with $\epsilon_{zz} = 0$ approximates better references [10] and [29] than $\epsilon_{zz} \neq 0$ as the authors use the $\epsilon_{zz} = 0$ approach. This study also lead us to conclude that the thickness stretching effect has influence on the buckling analysis of sandwich FGM plates as $\epsilon_{zz} = 0$ gives higher fundamental buckling loads than $\epsilon_{zz} \neq 0$.

The isotropic fully ceramic plate (first line on tables 12 and 13) has the higher fundamental buckling loads. As the core thickness to the total thickness of the plate ratio $((h_2 - h_1)/h)$ increases the buckling loads increase as well. This can be seen by looking at each line of the tables. Considering each column of both tables we may conclude that the critical buckling loads decrease as the power-law exponent p increases. From the comparison of tables 12 and 13 we deduce that the bi-axial buckling load of any simply supported sandwich square plate with FGM skins is half the uni-axial one for the same plate.

In figure 12 the first four buckling modes of a simply supported 2-1-2 sandwich square plate with FGM skins, $p = 0.5$, subjected to a uni-axial in-plane compressive load, using the higher-order plate theory and a grid with 17^2 points is presented. Figure 13 presents the first four buckling modes of a simply supported 2-1-1 sandwich square plate with FGM skins, $p = 10$, subjected to a bi-axial in-plane compressive load.

p	Theory	$\bar{P}$					
		1-0-1	2-1-2	2-1-1	1-1-1	2-2-1	1-2-1
0	CLPT	13.73791	13.73791	13.73791	13.73791	13.73791	13.73791
	FSDPT	13.00449	13.00449	13.00449	13.00449	13.00449	13.00449
	TSDPT [10]	13.00495	13.00495	13.00495	13.00495	13.00495	13.00495
	SSDPT [29]	13.00606	13.00606	13.00606	13.00606	13.00606	13.00606
	present $\epsilon_{zz} \neq 0$	12.95287	12.95287	12.95287	12.95287	12.95287	12.95287
	present $\epsilon_{zz} = 0$	13.00508	13.00508	13.00508	13.00508	13.00508	13.00508
0.5	CLPT	7.65398	8.25597	8.56223	8.78063	9.18254	9.61525
	FSDPT	7.33732	7.91320	8.20015	8.41034	8.78673	9.19517
	TSDPT [10]	7.36437	7.94084	8.22470	8.43645	8.80997	9.21681
	SSDPT [29]	7.36568	7.94195	8.22538	8.43712	8.81037	9.21670
	present $\epsilon_{zz} \neq 0$	7.16207	7.71627	7.98956	8.19278	8.55172	8.94190
	present $\epsilon_{zz} = 0$	7.18728	7.74326	8.01701	8.22133	8.58129	8.97310
1	CLPT	5.33248	6.02733	6.40391	6.68150	7.19663	7.78406
	FSDPT	5.14236	5.81379	6.17020	6.43892	6.92571	7.48365
	TSDPT [10]	5.16713	5.84006	6.19394	6.46474	6.94944	7.50656
	SSDPT [29]	5.16846	5.84119	6.19461	6.46539	6.94980	7.50629
	present $\epsilon_{zz} \neq 0$	5.06137	5.71135	6.05467	6.31500	6.78405	7.31995
	present $\epsilon_{zz} = 0$	5.07848	5.73022	6.07358	6.33556	6.80547	7.34367
5	CLPT	2.73080	3.10704	3.48418	3.65732	4.21238	4.85717
	FSDPT	2.63842	3.02252	3.38538	3.55958	4.09285	4.71475
	TSDPT [10]	2.65821	3.04257	3.40351	3.57956	4.11209	4.73469
	SSDPT [29]	2.66006	3.04406	3.40449	3.58063	4.11288	4.73488
	present $\epsilon_{zz} \neq 0$	2.63652	3.00791	3.36255	3.53005	4.05070	4.64701
	present $\epsilon_{zz} = 0$	2.64681	3.01865	3.37196	3.54148	4.06163	4.66059
10	CLPT	2.56985	2.80340	3.16427	3.25924	3.79238	4.38221
	FSDPT	2.46904	2.72626	3.07428	3.17521	3.68890	4.26040
	TSDPT [10]	2.48727	2.74632	3.09190	3.19471	3.70752	4.27991
	SSDPT [29]	2.48928	2.74844	3.13443	3.19456	3.14574	4.38175
	present $\epsilon_{zz} \neq 0$	2.47216	2.72046	3.06067	3.15761	3.66166	4.20550
	present $\epsilon_{zz} = 0$	2.48219	2.73080	3.06943	3.16837	3.67153	4.21792

Table 12
Uni-axial buckling load of simply supported plate of type C using the higher-order theory and a grid with 17^2 points.

p	Theory	$\bar{P}$					
		1-0-1	2-1-2	2-1-1	1-1-1	2-2-1	1-2-1
0	CLPT	6.86896	6.86896	6.86896	6.86896	6.86896	6.86896
	FSDPT	6.50224	6.50224	6.50224	6.50224	6.50224	6.50224
	TSDPT [10]	6.50248	6.50248	6.50248	6.50248	6.50248	6.50248
	SSDPT [29]	6.50303	6.50303	6.50303	6.50303	6.50303	6.50303
	present $\epsilon_{zz} \neq 0$	6.47643	6.47643	6.47643	6.47643	6.47643	6.47643
	present $\epsilon_{zz} = 0$	6.50254	6.50254	6.50254	6.50254	6.50254	6.50254
0.5	CLPT	3.82699	4.12798	4.28112	4.39032	4.59127	4.80762
	FSDPT	3.66866	3.95660	4.10007	4.20517	4.39336	4.59758
	TSDPT [10]	3.68219	3.97042	4.11235	4.21823	4.40499	4.60841
	SSDPT [29]	3.68284	3.97097	4.11269	4.21856	4.40519	4.60835
	present $\epsilon_{zz} \neq 0$	3.58104	3.85813	3.99478	4.09639	4.27586	4.47095
	present $\epsilon_{zz} = 0$	3.59364	3.87163	4.00851	4.11067	4.29064	4.48655
1	CLPT	2.66624	3.01366	3.20195	3.34075	3.59831	3.89203
	FSDPT	2.57118	2.90690	3.08510	3.21946	3.46286	3.74182
	TSDPT [10]	2.58357	2.92003	3.09697	3.23237	3.47472	3.75328
	SSDPT [29]	2.58423	2.92060	3.09731	3.23270	3.47490	3.75314
	present $\epsilon_{zz} \neq 0$	2.53069	2.85568	3.02733	3.15750	3.39202	3.65998
	present $\epsilon_{zz} = 0$	2.53924	2.86511	3.03679	3.16778	3.40274	3.67183
5	CLPT	1.36540	1.55352	1.74209	1.82866	2.10619	2.42859
	FSDPT	1.31921	1.51126	1.69269	1.77979	2.04642	2.35737
	TSDPT [10]	1.32910	1.52129	1.70176	1.78978	2.05605	2.36734
	SSDPT [29]	1.33003	1.52203	1.70224	1.79032	2.05644	2.36744
	present $\epsilon_{zz} \neq 0$	1.31826	1.50395	1.68128	1.76502	2.02535	2.32351
	present $\epsilon_{zz} = 0$	1.32340	1.50933	1.68598	1.77074	2.03081	2.33029
10	CLPT	1.28493	1.40170	1.58214	1.62962	1.89619	2.19111
	FSDPT	1.23452	1.36313	1.53714	1.58760	1.84445	2.13020
	TSDPT [10]	1.24363	1.37316	1.54595	1.59736	1.85376	2.13995
	SSDPT [29]	1.24475	1.37422	1.56721	1.59728	1.57287	2.19087
	present $\epsilon_{zz} \neq 0$	1.23608	1.36023	1.53034	1.57880	1.83083	2.10275
	present $\epsilon_{zz} = 0$	1.24109	1.36540	1.53472	1.58419	1.83576	2.10896

Table 13
Bi-axial buckling load of simply supported plate of type C using the higher-order theory and a grid with 17^2 points.

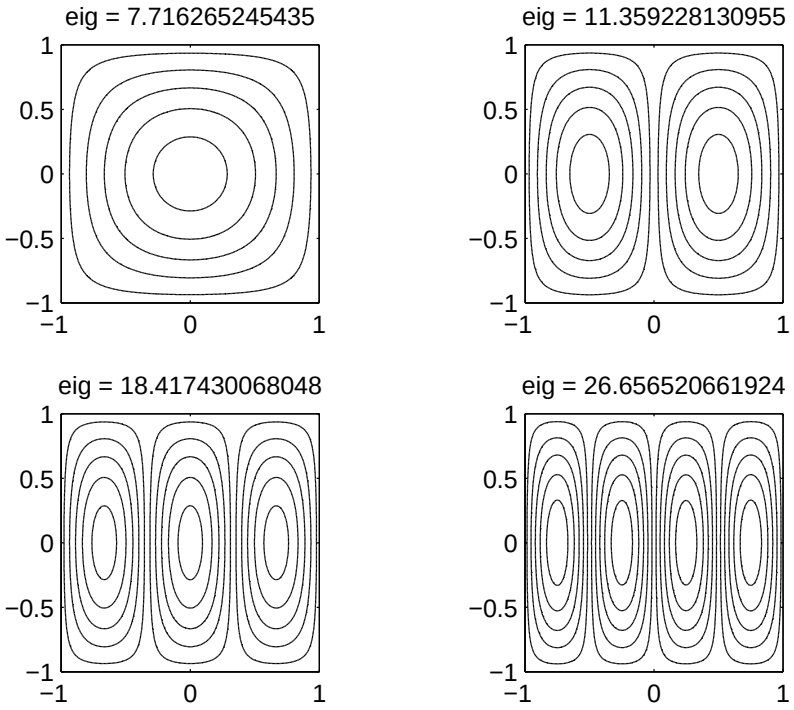

Fig. 12. First four buckling modes. Uni-axial buckling load of a simply supported 2-1-2 plate type C, $p = 0.5$, a 17^2 points grid, and using the higher-order theory.

7 Conclusions

A novel application of a Unified formulation coupled with collocation with radial basis functions is proposed. A thickness-stretching higher-order shear deformation theory was successfuly implemented for the static, free vibration, and linearized buckling analysis of functionally graded plates.

The present formulation was compared with analytical, meshless or finite element methods and proved very accurate in both static, vibration and buckling problems. The effect of $\epsilon_{zz} \neq 0$ showed significance in thicker plates. Even for a thinner functionally graded plate, the σ_{zz} should always be considered in the formulation.

For the first time, the complete governing equations and boundary conditions of the higher-order plate theory are presented to help readers to implement it successfully with the present or other strong-form techniques.

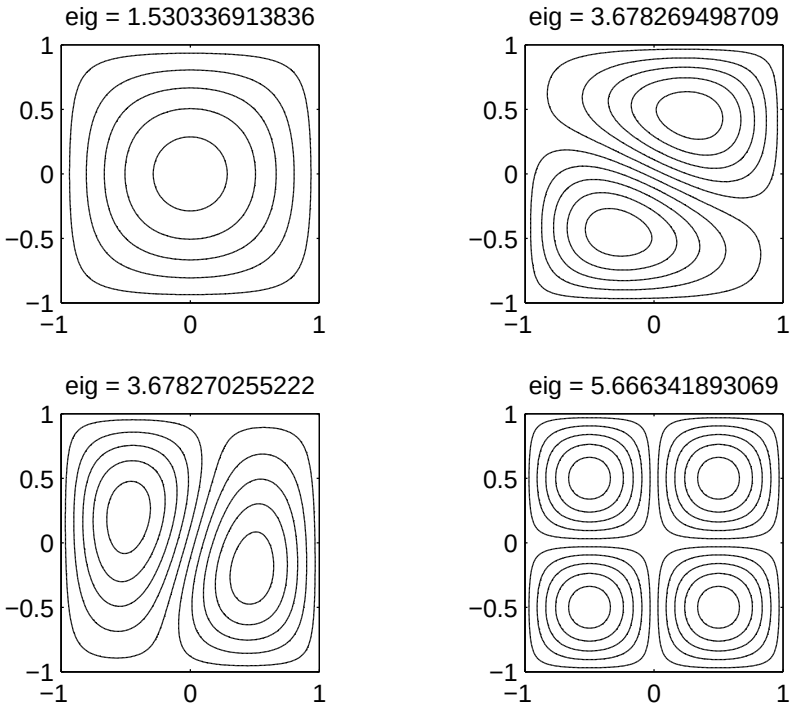

Fig. 13. First four buckling modes. Bi-axial buckling load of a simply supported 2-1-1 plate type C, $p = 10$, a 17^2 points grid, and using the higher-order theory.

Acknowledgments

The FCT support given to the first author under grant SFRH/BD/45554/2008 is acknowledged.

References

[1] M.B. Bever and P.E. Duwez. Gradients in composite materials. *Materials Science and Engineering*, 10(0):1 – 8, 1972.

[2] Y. Miyamoto, W.A. Kaysser, B.H. Rabin, A. Kawasaki, and R.G. Ford. *Functionally Graded Materials: Design, Processing and Applications*. Kluwer Academic Publishers, 1999.

[3] F.J. Ferrante and L.L. Graham-Brady. Stochastic simulation of non-gaussian/non-stationary properties in a functionally graded plate. *Computer Methods in Applied Mechanics and Engineering*, 194(12-16):1675 – 1692, 2005.

[4] H.M Yin, L.Z Sun, and G.H Paulino. Micromechanics-based elastic model for functionally graded materials with particle interactions. *Acta Materialia*, 52(12):3535 – 3543, 2004.

[5] Zheng Zhong and Ertao Shang. Closed-form solutions of three-dimensional functionally graded plates. *Mechanics of Advanced Materials and Structures*, 15(5):355–363, 2008.

[6] T. K. Nguyen, K. Sab, and G. Bonnet. Shear correction factors for functionally graded plates. *Mechanics of Advanced Materials and Structures*, 14(8):567–575, 2007.

[7] Victor Birman and Larry W. Byrd. Modeling and analysis of functionally graded materials and structures. *Applied Mechanics Reviews*, 60(5):195–216, 2007.

[8] M. Koizumi. Fgm activities in japan. *Composites Part B: Engineering*, 28(1-2):1 – 4, 1997. Use of Composites Multi-Phased and Functionally Graded Materials.

[9] J. N. Reddy and C. D. Chin. Thermomechanical analysis of functionally graded cylinders and plates. *Journal of Thermal Stresses*, 21(6):593–626, 1998.

[10] J. N. Reddy. Analysis of functionally graded plates. *International Journal for Numerical Methods in Engineering*, 47:663–684, 2000.

[11] S. S. Vel and R. C. Batra. Three-dimensional analysis of transient thermal stresses in functionally-graded plates. *International Journal of Solids and Structures*, in press, 2003.

[12] S. S. Vel and R. C. Batra. Exact solution for thermoelastic deformations of functionally graded thick rectangular plates. *AIAA Journal*, 40:1421–1433, 2002.

[13] Z. Q. Cheng and R. C. Batra. Three-dimensional thermoelastic deformations of a functionally graded-elliptic plate. *Composites: Part B*, 31:97–106, 2000.

[14] Javaheri R. and Eslami M. R. Thermal buckling of functionally graded plates based on higher order theory. *Journal of Thermal Stresses*, 25(7):603–625, 2002.

[15] M. Kashtalyan. Three-dimensional elasticity solution for bending of functionally graded rectangular plates. *European Journal of Mechanics - A/Solids*, 23(5):853 – 864, 2004.

[16] M. Kashtalyan and M. Menshykova. Three-dimensional elasticity solution for sandwich panels with a functionally graded core. *Composite Structures*, 87(1):36 – 43, 2009.

[17] L. F. Qian, R. C. Batra, and L. M. Chen. Static and dynamic deformations of thick functionally graded elastic plate by using higher-order shear and normal deformable plate theory and meshless local petrov-galerkin method. *Composites: Part B*, 35:685–697, 2004.

[18] A.M. Zenkour. A comprehensive analysis of functionally graded sandwich plates: Part 1–deflection and stresses. *International Journal of Solids and Structures*, 42(18-19):5224 – 5242, 2005.

[19] A. M. Zenkour. Generalized shear deformation theory for bending analysis of functionally graded plates. *Appl Math Modell*, 30:67–84, 2006.

[20] Fernando Ramirez, Paul R. Heyliger, and Ernian Pan. Static analysis of functionally graded elastic anisotropic plates using a discrete layer approach. *Composites Part B: Engineering*, 37(1):10 – 20, 2006.

[21] A. J. M. Ferreira, R. C. Batra, C. M. C. Roque, L. F. Qian, and P. A. L. S. Martins. Static analysis of functionally graded plates using third-order shear deformation theory and a meshless method. *Composite Structures*, 69(4):449–457, 2005.

[22] A. J. M. Ferreira, C. M. C. Roque, R. M. N. Jorge, G. E. Fasshauer, and R. C. Batra. Analysis of functionally graded plates by a robust meshless method. *Mechanics of Advanced Materials and Structures*, 14(8):577–587, 2007.

[23] Shyang-Ho Chi and Yen-Ling Chung. Mechanical behavior of functionally graded material plates under transverse load–part i: Analysis. *International Journal of Solids and Structures*, 43(13):3657 – 3674, 2006.

[24] Shyang-Ho Chi and Yen-Ling Chung. Mechanical behavior of functionally graded material plates under transverse load–part ii: Numerical results. *International Journal of Solids and Structures*, 43(13):3675 – 3691, 2006.

[25] Z. Q. Cheng and R. C. Batra. Deflection relationships between the homogeneous kirchhoff plate theory and different functionally graded plate theories. *Archive of Mechanics*, 52:143–158, 2000.

[26] R.C. Batra and J. Jin. Natural frequencies of a functionally graded anisotropic rectangular plate. *Journal of Sound and Vibration*, 282(1-2):509 – 516, 2005.

[27] A. J. M. Ferreira, R. C. Batra, C. M. C. Roque, L. F. Qian, and R. M. N. Jorge. Natural frequencies of functionally graded plates by a meshless method. *Composite Structures*, 75(1-4):593–600, September 2006.

[28] S. S. Vel and R. C. Batra. Three-dimensional exact solution for the vibration of functionally graded rectangular plates. *Journal of Sound and Vibration*, 272:703–730, 2004.

[29] A.M. Zenkour. A comprehensive analysis of functionally graded sandwich plates: Part 2–buckling and free vibration. *International Journal of Solids and Structures*, 42(18-19):5243 – 5258, 2005.

[30] C.M.C. Roque, A.J.M. Ferreira, and R.M.N. Jorge. A radial basis function approach for the free vibration analysis of functionally graded plates using a refined theory. *Journal of Sound and Vibration*, 300(3-5):1048 – 1070, 2007.

[31] Z. Q. Cheng and R. C. Batra. Exact correspondence between eigenvalues of membranes and functionally graded simply supported polygonal plates. *Journal of Sound and Vibration*, 229:879–895, 2000.

[32] M. M. Najafizadeh and M. R. Eslami. Buckling analysis of circular plates of functionally graded materials under uniform radial compression. *International Journal of Mechanical Sciences*, 44(12):2479 – 2493, 2002.

[33] V. Birman. Buckling of functionally graded hybrid composite plates. *Proceedings of the 10th Conference on Engineering Mechanics*, pages 1199–1202, 1995.

[34] R. Javaheri and M.R. Eslami. Buckling of functionally graded plates under in-plane compressive loading. *ZAMM - Journal of Applied Mathematics and Mechanics / Zeitschrift fÃijr Angewandte Mathematik und Mechanik*, 82(4):277–283, 2002.

[35] T. Kant, D. R. J. Owen, and O. C. Zienkiewicz. A refined higher-order c^o plate element. *Computers and Structures*, 15(2):177–183, 1982.

[36] B. N. Pandya and T. Kant. Higher-order shear deformable theories for flexure of sandwich plates–finite element evaluations. *International Journal of Solids and Structures*, 24(12):1267–1286, 1988.

[37] B. N. Pandya and T. Kant. Finite element analysis of laminated composite plates using a higher-order displacement model. *Composites Science and Technology*, 32(2):137–155, 1988.

[38] T. Kant and K. Swaminathan. Analytical solutions for the static analysis of laminated composite and sandwich plates based on a higher order refined theory. *Composite Structures*, 56(4):329 – 344, 2002.

[39] T. Kant and K. Swaminathan. Analytical solutions for free vibration of laminated composite and sandwich plates based on a higher-order refined theory. *Composite Structures*, 53(1):73 – 85, 2001.

[40] Ajay Kumar Garg, Rakesh Kumar Khare, and Tarun Kant. Higher-order closed-form solutions for free vibration of laminated composite and sandwich shells. *Journal of Sandwich Structures and Materials*, 8(3):205–235, 2006.

[41] E. Carrera. Evaluation of layer-wise mixed theories for laminated plate analysis. *AIAA Journal*, (36):830–839, 1998.

[42] E. Carrera. Developments, ideas, and evaluations based upon reissner's mixed variational theorem in the modelling of multilayered plates and shells. *Applied Mechanics Reviews*, 54:301–329, 2001.

[43] Erasmo Carrera. Theories and finite elements for multilayered plates and shells: A unified compact formulation with numerical assessment and benchmarking. *Archives of Computational Methods in Engineering*, 10:215–296.

[44] S. Brischetto and E. Carrera. Advanced mixed theories for bending analysis of functionally graded plates. *Computers and Structures*, 88(23-24):1474 – 1483, 2010.

[45] S. Brischetto. Classical and mixed advanced models for sandwich plates embedding functionally graded cores. *J Mech Mater Struct*, 4:13–33, 2009.

[46] E. Carrera, S. Brischetto, and A. Robaldo. Variable kinematic model for the analysis of functionally graded material plates. *AIAA Journal*, 46:194–203, 2008.

[47] E. Carrera, S. Brischetto, M. Cinefra, and M. Soave. Effects of thickness stretching in functionally graded plates and shells. *Composites Part B: Engineering*, 42:123–133, 2011.

[48] A. J. M. Ferreira. A formulation of the multiquadric radial basis function method for the analysis of laminated composite plates. *Composite Structures*, 59:385–392, 2003.

[49] A. J. M. Ferreira. Thick composite beam analysis using a global meshless approximation based on radial basis functions. *Mechanics of Advanced Materials and Structures*, 10:271–284, 2003.

[50] A. J. M. Ferreira, C. M. C. Roque, and P. A. L. S. Martins. Analysis of composite plates using higher-order shear deformation theory and a finite point formulation based on the multiquadric radial basis function method. *Composites: Part B*, 34:627–636, 2003.

[51] A.J.M. Ferreira, C.M.C. Roque, R.M.N. Jorge, and E.J. Kansa. Static deformations and vibration analysis of composite and sandwich plates using a layerwise theory and multiquadrics discretizations. *Engineering Analysis with Boundary Elements*, 29(12):1104 – 1114, 2005.

[52] A.J.M. Ferreira, C.M.C. Roque, and R.M.N. Jorge. Analysis of composite plates by trigonometric shear deformation theory and multiquadrics. *Computers & Structures*, 83(27):2225 – 2237, 2005.

[53] A.J.M. Ferreira, R.C. Batra, C.M.C. Roque, L.F. Qian, and R.M.N. Jorge. Natural frequencies of functionally graded plates by a meshless method. *Composite Structures*, 75(1-4):593 – 600, 2006.

[54] A.J.M. Ferreira, C.M.C. Roque, and R.M.N. Jorge. Free vibration analysis of symmetric laminated composite plates by fsdt and radial basis functions. *Computer Methods in Applied Mechanics and Engineering*, 194(39-41):4265 – 4278, 2005.

[55] A. J. M. Ferreira, C. M. C. Roque, and P. A. L. S. Martins. Radial basis functions and higher-order shear deformation theories in the analysis of laminated composite beams and plates. *Composite Structures*, 66(1-4):287 – 293, 2004.

[56] A.J.M. Ferreira, C.M.C. Roque, E. Carrera, M. Cinefra, and O. Polit. Radial basis functions collocation and a unified formulation for bending, vibration and buckling analysis of laminated plates, according to a variation of murakamiâĂŹs zig-zag theory. *European Journal of Mechanics - A/Solids*, 30(4):559 – 570, 2011.

[57] J.D. Rodrigues, C.M.C. Roque, A.J.M. Ferreira, E. Carrera, and M. Cinefra. Radial basis functions-finite differences collocation and a unified formulation for bending, vibration and buckling analysis of laminated plates, according to murakami's zig-zag theory. *Composite Structures*, 93(7):1613 – 1620, 2011.

[58] A.J.M. Ferreira, C.M.C. Roque, E. Carrera, and M. Cinefra. Analysis of thick isotropic and cross-ply laminated plates by radial basis functions and a unified formulation. *Journal of Sound and Vibration*, 330(4):771 – 787, 2011.

[59] A. J.M. Ferreira, C. M.C. Roque, E. Carrera, M. Cinefra, and O. Polit. Two higher order zig-zag theories for the accurate analysis of bending, vibration and buckling response of laminated plates by radial basis functions collocation and a unified formulation. *Journal of Composite Materials*, 2011.

[60] A.M.A. Neves, A.J.M. Ferreira, E. Carrera, C.M.C. Roque, M. Cinefra, R.M.N. Jorge, and C.M.M. Soares. Bending of fgm plates by a sinusoidal plate formulation and collocation with radial basis functions. *Mechanics Research Communications*, 38(5):368 – 371, 2011.

[61] A.M.A. Neves, A.J.M. Ferreira, E. Carrera, C.M.C. Roque, M. Cinefra, R. M.N. Jorge, and C.M.M. Soares. A quasi-3d sinusoidal shear deformation theory for the static and free vibration analysis of functionally graded plates. *Composites Part B*, In Press, Accepted Manuscript:–, 2011.

[62] E. Carrera. C^0 reissner-mindlin multilayered plate elements including zig-zag and interlaminar stress continuity. *International Journal of Numerical Methods in Engineering*, 39:1797–1820, 1996.

[63] T Mori and K Tanaka. Average stress in matrix and average elastic energy of materials with misfitting inclusions. *Acta Metallurgica*, 21(5):571 – 574, 1973.

[64] Y. and Benveniste. A new approach to the application of mori-tanaka's theory in composite materials. *Mechanics of Materials*, 6(2):147 – 157, 1987.

[65] R. L. Hardy. Multiquadric equations of topography and other irregular surfaces. *Geophysical Research*, 176:1905–1915, 1971.

[66] E. J. Kansa. Multiquadrics- a scattered data approximation scheme with applications to computational fluid dynamics. i: Surface approximations and partial derivative estimates. *Computers and Mathematics with Applications*, 19(8/9):127–145, 1990.

[67] H. Wendland. Error estimates for interpolation by compactly supported radial basis functions of minimal degree. *J. Approx. Theory*, 93:258–296, 1998.

[68] A. J. M. Ferreira and G. E. Fasshauer. Computation of natural frequencies of shear deformable beams and plates by a rbf-pseudospectral method. *Computer Methods in Applied Mechanics and Engineering*, 196:134–146, 2006.

[69] S. S. Vel and R. C. Batra. Three-dimensional exact solution for the vibration of functionally graded rectangular plates. *Journal of Sound and Vibration*, 272:703–730, 2004.

[70] L. F. Qian, R. C. Batra, and L. M. Chen. Static and dynamic deformations of thick functionally graded elastic plate by using higher-order shear and normal deformable plate theory and meshless local petrov-galerkin method. *Composites: Part B*, 35:685–697, 2004.